Biogeosciences, 13, 2029–2049, 2016
www.biogeosciences.net/13/2029/2016/
doi:10.5194/bg-13-2029-2016

Biogeosciences Open Access EGU

Seasonal variations in metallic mercury (Hg^0) vapor exchange over biannual wheat–corn rotation cropland in the North China Plain

Jonas Sommar[1], Wei Zhu[1,a], Lihai Shang[1], Che-Jen Lin[1,2], and Xinbin Feng[1]

[1]State Key Laboratory of Environmental Geochemistry, Institute of Geochemistry, Chinese Academy of Sciences, Guiyang 550002, China
[2]Center for Advances in Water and Air Quality, Lamar University, Beaumont, TX 77710, USA
[a]now at: Department of Chemistry, Umeå University, 901 87 Umeå, Sweden

Correspondence to: Jonas Sommar (jonas@mail.gyig.ac.cn) and Xinbin Feng (fengxinbin@vip.skleg.cn)

Received: 10 September 2015 – Published in Biogeosciences Discuss.: 30 September 2015
Revised: 3 March 2016 – Accepted: 21 March 2016 – Published: 7 April 2016

Abstract. Air–surface gas exchange of Hg^0 was measured in five approximately bi-weekly campaigns (in total 87 days) over a wheat–corn rotation cropland located on the North China Plain (NCP) using the relaxed eddy accumulation (REA) technique. The campaigns were separated over the duration of a full-year period (2012–2013) aiming to capture the flux pattern over essential growing stages of the planting system with a low homogeneous topsoil Hg content ($\sim 45\,ng\,g^{-1}$). Contrasting pollution regimes influenced air masses at the site and corresponding Hg^0 concentration means (3.3 in late summer to $6.2\,ng\,m^{-3}$ in winter) were unanimously above the typical hemispheric background of 1.5–$1.7\,ng\,m^{-3}$ during the campaigns. Extreme values in bi-directional net Hg^0 exchange were primarily observed during episodes of peaking Hg^0 concentrations. In tandem with under-canopy chamber measurements, the above-canopy REA measurements provided evidence for a balance between Hg^0 ground emissions and uptake of Hg^0 by the developed canopies. During the wheat growing season covering $\sim 2/3$ of the year at the site, net field-scale Hg^0 emission prevailed for periods of active plant growth until canopy senescence (mean flux: $20.0\,ng\,m^{-3}$), showing the dominance of Hg^0 soil efflux during warmer seasons. In the final vegetative stage of corn and wheat, ground and above-canopy Hg^0 flux displayed inversed daytime courses with a near mid-day maximum (emission) and minimum (deposition), respectively. In contrast to wheat, Hg^0 uptake of the corn canopy at this stage offset ground Hg^0 emissions with additional removal of Hg^0 from the atmosphere. Differential uptake of Hg^0 between wheat (C_3 species) and corn (C_4 species) foliage is discernible from estimated Hg^0 flux (per leaf area) and Hg content in mature cereal leaves, being a factor of > 3 higher for wheat (at $\sim 120\,ng\,g^{-1}$ dry weight). Furthermore, this study shows that intermittent flood irrigation of the air-dry field induced a short pulse of Hg^0 emission due to displacement of Hg^0 present in the surface soil horizon. A more lingering effect of flood irrigation is however suppressed Hg^0 soil emissions, which for wet soil (~ 30 % vol) beneath the corn canopy was on average a factor of ~ 3 lower than that for drier soil (< 10 % vol) within wheat stands. Extrapolation of the campaign Hg^0 flux data (mean: $7.1\,ng\,m^{-2}\,h^{-1}$) to the whole year suggests the wheat–corn rotation cropland to be a net source of atmospheric Hg^0. The observed magnitude of annual wet deposition flux ($\sim 8.8\,\mu g\,Hg\,m^{-2}$) accounted for a minor fraction of soil Hg^0 evasion flux prevailing over the majority of the year. Therefore, we suggest that dry deposition of other forms of airborne Hg constitutes the dominant pathway of Hg input to this local ecosystem and that these deposited forms would be gradually transformed and re-emitted as Hg^0 rather than being sequestered here. In addition, after crop harvesting, the practice of burning agricultural residue with considerable Hg content rather than straw return management yields seasonally substantial atmospheric Hg^0 emissions from croplands in the NCP region.

Published by Copernicus Publications on behalf of the European Geosciences Union.

1 Introduction

Mercury (Hg) is an important environmental contaminant because of its cyclic transport between air, water, soil and the biosphere and its tendency to bioaccumulate in the environment as neurotoxic mono-methylated (CH_3Hg-) compounds (Driscoll et al., 2013). While assessments of Hg burden in environmental compartments are rather concordant, the fluxes between them are less well constrained (Selin, 2009) and specifically concern land ecosystem–atmosphere exchange of Hg^0 (Zhang et al., 2012). Hg in the biosphere is derived primarily from atmospheric deposition (Grigal, 2003), where foliar uptake of Hg^0 has been recognized as a principal pathway for atmospheric Hg to enter terrestrial ecosystems (Frescholtz et al., 2003; Niu et al., 2011; Obrist, 2007). In turn, the availability of soil (inorganic) mercury to aerial parts of terrestrial plants is generally low and the uptake is mainly retained in the root zone (Cavallini et al., 1999; Meng et al., 2010; Cui et al., 2014). Accumulated Hg in foliage is transferred to soil reservoirs via plant detritus (St Louis et al., 2001) or may partially be released back into the atmosphere (Bash and Miller, 2009). In addition, Hg may enter the foliage by recycling processes, releasing Hg^0 from underlying soil surfaces (Millhollen et al., 2006). In a review (Sommar et al., 2013a), the majority of reported Hg^0 flux measurements over terrestrial soils indicate net emission in warmer seasons and near-zero fluxes at cold temperatures. Soil–air Hg^0 exchange is controlled by numerous factors including physico-chemical properties of and abiotic/biotic processes in the soil, meteorological conditions and atmospheric composition (Bahlmann et al., 2006; Carpi and Lindberg, 1997; Engle et al., 2005; Fritsche et al., 2008a; Gustin, 2011; Rinklebe et al., 2010; Mauclair et al., 2008; Zhang et al., 2008). For bare low Hg-containing soils, Briggs and Gustin (2013) proposed a conceptual model in which the soil moisture regimes largely dictate the level of Hg^0 flux. The presence of vegetation has an effect on the Hg^0 efflux from ground surfaces by modifying soil moisture by evapotranspiration as well as reducing light penetration, soil temperature and air mixing.

At landscape scale, Hg^0 net exchange measurements may be made directly, using micrometeorological (MM) methods above vegetation canopies (Bash and Miller, 2009; Baya and Van Heyst, 2010; Cobos et al., 2002; Converse et al., 2010; Edwards et al., 2005; Fritsche et al., 2008b; Kim et al., 1995; Marsik et al., 2005; Sommar et al., 2013b). As for numerous trace gases (Fowler et al., 2009), the exchange fluxes of Hg^0 vary in sign and magnitude (bi-directional exchange). From MM-flux measurements covering larger temporal scales, it is inferred that vegetated ecosystems can represent both a source and a sink for Hg^0 over shorter or longer periods, depending on the atmospheric concentration, meteorology, substrates, climate conditions and plant community composition (Bash and Miller, 2009; Converse et al., 2010; Lee et al., 2000). However, related Hg^0 flux measurements over managed ecosystems, such as croplands, are sparse and only at best seasonally resolved (Baya and Van Heyst, 2010). Broader seasonal flux data sets are desirable, since the annual net Hg^0 flux over an ecosystem may represent a subtle balance between opposing processes (Lee et al., 2000). The assessment of local Hg balances in agricultural regions is challenging, since during a year, very different and contrasted conditions are observed from the fallow period to the maximum development of a crop. The foliar uptake of Hg^0 by major staple grain crops has been studied at low–moderate (Niu et al., 2011) and high exposure treatments of Hg^0 vapor (Browne and Fang, 1978; Du and Fang, 1982). The early work conducted on cereals at the tillering stage suggested that assimilation of Hg^0 increased with Hg^0 concentration, temperature and irradiation, and is controlled by interior (mesophyll) resistances at optimal growing conditions. The study of Niu et al. (2011) focusing on wheat and corn indicated a significant correlation between foliage Hg content and the exposure level of airborne Hg^0 for their principal growing stages. In a further study, Niu et al. (2014) showed that only a moderate level of Hg^0 pollution in air ($\sim 20\,ng\,m^{-3}$) was required to induce measurable physiological stress on corn tissue.

China is the largest emitter of atmospheric Hg worldwide due to a rapid expansion in fossil fuel combustion (one quarter of global coal combustion) and increased industrialization, in contrast to significant reduction in anthropogenic emissions in Europe and North America (Streets et al., 2005). In addition, China is the world's leading producer and consumer of Hg (USGS, 2015). Using a broad set of [Hg^0] / [CO]-ratio observations, Fu et al. (2015) recently estimated the annual anthropogenic Hg^0 emission in mainland China to be approximately 1140 ton, which is significantly higher than previously predicted by published emission inventories using activity data (S. Wang et al., 2014). This inconsistency also inferred by Song et al. (2015) may propagate into biased-low source strength estimates or missing source categories in inventories. Since the elevated Hg deposition deriving from anthropogenic sources tends to concentrate in labile pools, the potential for high re-emission of Hg^0 from impacted terrestrial ecosystems in China is substantial (Fu et al., 2012; Smith-Downey et al., 2010). Investigations by the dynamic flux chamber (DFC) technique have revealed comparatively high Hg^0 efflux from agricultural soils compared to soils in other types of land use in China (Fu et al., 2008, 2012; Wang et al., 2006; Zhu et al., 2011; Zhu et al., 2015a). Therefore, it may be hypothesized for related croplands that Hg^0 emissions from the soil surface, though plausibly (in part) recaptured by uptake of the overlying canopy, at times have a major contribution to the net Hg^0 exchange, especially in scant or senescent canopies. Micrometeorological measurements yielding the net flux from the canopy surface, including both soil and plant exchanges, are thus required to address the importance of cropland and other agroecosystems as sources/sinks of Hg^0. In an effort to investigate Hg^0 uptake or emission from crop vegetation and soil,

we have conducted broad seasonal measurements of field-scale Hg^0 flux at three sites in distinctively different agricultural regions of China with varying levels of Hg content in agricultural soil. All the selected sites were located in a rural environment without discernible adjacent anthropogenic Hg point sources. The well-characterized and typical rotation croplands investigated include either paddy or dry land cultivation only or a combination thereof over a year. We focus on the four cash crops (rice, wheat, corn, and oilseed rape) accounting for the bulk of the planting area in mainland China. In order to determine the origin of fluxes, we combined large-scale above-canopy MM-method flux techniques with small-scale automated DFC measurement at the canopy floor in the field experiments. In this paper, we report on Hg^0 flux measurements in and above a farm field growing winter wheat and summer corn in rotation during five campaigns (overall 87 sampling days) over the period May 2012 to April 2013. The site is located on the central North China Plain (NCP, between 32–40° N and 114–121° E), which is considered to be China's granary (covering about 180 000 km^2 of farmlands) with about half and a third of the national wheat and corn production, respectively (NBSC, 1998). Besides being a major agricultural base, the NCP region is heavily populated and industrialized and suffers from serious particulate and photochemical air pollution (L. T. Wang et al., 2014; Wen et al., 2015). Forthcoming communications will deal with characteristics of Hg^0 fluxes measured over subtropical croplands growing either oilseed rape or rice in rotation or rice as a single crop. Jointly, in these papers, we present growing and non-growing season Hg^0 flux patterns and diurnal features. In addition, we address the role of crop vegetation as a source/sink of Hg^0 based on an analysis of the measured difference between above-canopy and ground Hg^0 fluxes. We also attempt to address the impact of field management activities (e.g., harvest, tillering and irrigation) and abrupt changes in environmental conditions (e.g., intensive precipitation) on Hg^0 gas exchange.

2 Materials and methods

2.1 Site description

The Yucheng Comprehensive Experimental Station (YCES, 36°57′ N, 116°36′ E, managed by the Chinese Academy of Sciences) experimental site is located on an alluvial plain in the lower reaches of the Yellow River, Shandong province, China. There is a typical crop rotation of winter wheat and summer corn in the region without fallow between the crops. The annual mean air temperature and precipitation depth were 12.9 ± 0.8 °C and 528 ± 197 mm, respectively, for 2003–2012 (Bao et al., 2014). Due to the East Asia monsoon, the precipitation pattern is largely asymmetric, with 60–70 % of the total concentrated in July–August. The wheat-growing season (mean length: 237 ± 8 days) is characterized as dry, windy and with less precipitation

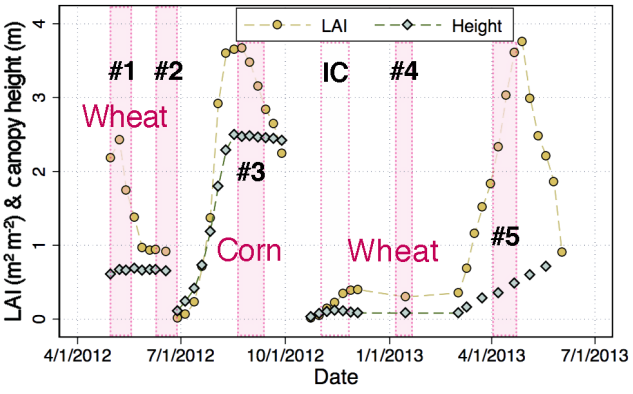

Figure 1. Seasonal variation in LAI ($m^2\ m^{-2}$, yellow filled circles) and canopy height (green filled diamonds) for 2012–2013 (in part). The duration of the five flux sampling periods (with numbers given in consecutive order) is indicated by magenta shaded boxes. The grey box resembles the time duration of a field inter-comparison (IC) of chamber and micrometeorological flux measurement techniques to quantify Hg^0 flux (Zhu et al., 2015a).

(108 ± 238 mm), whereas the corn-growing season (mean length: 107 ± 7 days) is generally categorized as semi-humid and warm temperate. The upper texture of farmland soil is a silty loam with a volumetric soil water content at a field capacity of 0.44 $m^3\ m^{-3}$ (Li et al., 2010). In the tillage layer, the soil organic content is 1.21 % and the pH value is about 7.9 (Tong et al., 2014). Especially for winter wheat, precipitation does not meet crop water demand, so the cropland is flood irrigated using groundwater during the pre-frost, jointing, and shooting stages of wheat and prior to planting corn (typically ~ 100 mm per turn). For the period of this field study (May 2012 to April 2013, Fig. 1), the harvest and sowing dates of wheat were on 24 June and 11 October, respectively. In turn, corn was planted on 28 June with a density at 65 000 plants ha^{-1} and harvested on 5 October. Row spacing was ~ 25 cm and the direction was north–south. The total Hg (THg) content in surface soils was uniform across the measurement fetch (mean: 45 ± 3 ng g^{-1}, $n = 29$; Sommar et al., 2013b).

2.2 Micrometeorological flux measurements and calculations

The site was in the center of a flat ~ 15 ha grain field and a minimum fetch length of at least 130 m in all directions (Sommar et al., 2013b). From a 6.5 m high flux tower erected permanently over a year-long period, MM flux measurements were conducted. Sensible heat (H^{EC}), latent heat (λE^{EC}) and CO_2 fluxes ($F^{EC}_{CO_2}$) were measured by the eddy covariance (EC) method using the instrumentation and protocol described in Sommar et al. (2013b) and Zhu et al. (2015a, b). In order to diminish frequency response errors, the EC sensor height was adjusted over time (2.1–4.2 m) to keep a relative height between sensors and the canopy of

at least ∼ 1.5 m during a campaign (Burba, 2013). The frequency response of the sensor placement over the canopy was investigated by spectral analysis of selected 10 Hz turbulence time series. Analogous to that reported in Sommar et al. (2013b), there was over time little contribution from small eddies occurring above 5 Hz, and instrumentation produced in general co-spectra similar to the references (Kaimal et al., 1972).

Up to now, fast high-precision detectors for direct background Hg^0 flux measurements by the preferred EC method have not been available. A principal alternative flux measurement approach is the relaxed eddy accumulation (REA) technique (Businger and Oncley, 1990). As in EC, REA measurements are performed at a single point above the surface, but the detector required in EC is substituted by fast-response sampling valves. The inlet of an Hg^0–REA system was installed at the same height as the EC sensors, with a horizontal displacement distance to the EC sensors of 20 cm. The design and operation of the whole-air Hg^0–REA system used in this study has been described in detail by Sommar et al. (2013b). The REA system was specifically adapted to an automatic Hg^0 vapor analyzer (model 2537B, Tekran Instruments Inc.) to measure fluxes and concentrations of Hg^0. In this system, upward and downward moving air created from eddies in the air column are sampled and separated into reservoirs by the sampling valves. Updraft and downdraft sampling conditions are dictated by $w > \bar{w} + 0.3\bar{\sigma}_w$ and $w < \bar{w} - 0.3\bar{\sigma}_w$, respectively, where $\bar{w}$ is the 5 min running average of w and $\bar{\sigma}_w$ is the standard deviation of w over the same interval. Hg^0 flux (F^{REA}) is determined over 20 min sampling intervals following

$$F^{\mathrm{REA}} = \beta_{T_s} \cdot \sigma_w \cdot \underbrace{\left(\overline{C^{\uparrow}} - \overline{C^{\downarrow}}\right)}_{\Delta C_{\mathrm{REA}}}, \quad (1)$$

where σ_w (m s^{-1}) is the standard deviation of w, and $\overline{C^{\uparrow}}$ and $\overline{C^{\downarrow}}$ are the average mass concentrations of Hg^0 (at standard temperature and pressure) from updraft and downdraft samples corrected for dilution by zero air injection, respectively (ng m^{-3}). In turn, the empirical dimensionless parameter β_{T_s} was calculated online for each averaging period (20 min) according to

$$\beta_{T_s} = \overline{w'T_s'} \Big/ \left[\sigma_w \cdot \left(\overline{T_s^{\uparrow}} - \overline{T_s^{\downarrow}}\right)\right], \quad (2)$$

where T_s is temperature measured by the sonic anemometer of the EC system (K), $\overline{w'T_s'}$ is the kinematic buoyancy flux derived from EC (K m s^{-1}) and $\overline{T_s^{\uparrow}} - \overline{T_s^{\downarrow}}$ ($\Delta T_{s,\,\mathrm{REA}}$) is the average T_s difference in between updraft and downdraft samples (K). If the online calculated β_{T_s} deviated outside a ±0.2 interval of the median, the overall median value (0.46) was implemented in Eq. (1).

Bulk canopy conductance for water vapor, g_c (m s^{-1}), was estimated using a rearranged form of the Penman–Monteith equation (Dengel and Grace, 2010):

$$g_c = \left\{\left[\left(\frac{\Delta}{\gamma}\right) \cdot \left(\frac{H^{\mathrm{EC}}}{\lambda E^{\mathrm{EC}}}\right) - 1\right] \cdot (1/g_a) + \left(\frac{\rho_a \cdot c_p}{\gamma}\right) \cdot \left(\frac{D_a}{\lambda E^{\mathrm{EC}}}\right)\right\}^{-1}, \quad (3)$$

where Δ is the rate of the increase in saturation vapor pressure with air temperature (kPa K^{-1}), γ the psychrometric constant (kPa K^{-1}), g_a is the aerodynamic conductance (m s^{-1}), ρ_a the density of dry air (mol m^{-3}), c_p the specific heat of air (J mol^{-1} K^{-1}), and D_a the water vapor saturation deficit (kPa). Aerodynamic conductance was estimated following Thom (1975):

$$g_a = \kappa^2 \cdot u / \left[\ln\left((z-d)/z_0\right)\right]^2, \quad (4)$$

where κ is the von Kármán constant (0.41) and u is the wind speed measured at height z (m s^{-1}). z_0 is the surface roughness ($0.15 \cdot h_c$, where h_c is the mean canopy height) and d the zero plane displacement ($0.67 \cdot h_c$). In dry, daytime conditions most of the water vapor flux E^{EC} would derive from stomata, with only minor contributions from soil and leaf surface evaporation. Consequently, we only choose daytime conditions (global radiation > 100 W m^{-2}) without the presence of a wet canopy to calculate g_c as a proxy for canopy stomatal conductance. Most of the data were collected under favorable weather conditions without rainfall and with sufficient global radiation. However, as only a limited set of g_c data was obtained from the winter campaign due to wetness constraints and instrumentation malfunction, these data were not included in any further evaluation (cf. Table 1).

2.3 Ancillary measurements

The REA-EC instrumentation was accompanied by an automatic weather station (HOBO U30-NRC, Onset Computer Corp., USA) equipped with sensors for bulk air (temperature and humidity) and surface soil (temperature and volumetric moisture content) parameters and leaf wetness as well as sensors for global radiation (300–1100 nm) and photosynthetically active radiation (PAR, 400–700 nm), respectively. The weather station stored data as 20 min averages with the same time interval as the flux measurements. Crop leaf area index (LAI) was measured using an area meter (LI-3100, LI-COR Biosciences) weekly during the growing season. h_c was recorded at the same time interval. For the measurement campaigns with developed canopies (1–3; See Table 1), concurrent measurements of both above-canopy Hg^0 net exchange by the REA system as well as canopy-floor air–soil exchange by a dynamic flux chamber (DFC, Lin et al., 2012) were conducted with 20 min time resolution. The setup and operation of the automatic DFC system have been described elsewhere (Zhu et al., 2015a). Measurement results of air–soil Hg^0 flux are briefly provided here in connection with the discussion of MM-derived Hg^0 fluxes. Corn and wheat foliage samples were collected at harvest stage and analyzed

Table 1. Summary of turbulent Hg^0 fluxes measured by the REA technique, micrometeorological parameters measured by EC and auxiliary meteorological and environmental observations (presented as 20 min averages) during the five campaigns.

Variable	Unit	1 (2–18 May 2012)		2 (12–29 Jun 2012)		3 (29 Aug–17 Sep 2012)		4 (12–24 Jan 2013)		5 (1–24 April 2013)	
		Wheat, ∼ 65–70 cm, LAI ∼ 2.4–1.0		Wheat, ∼ 70 cm,	LAI < 1.0	Corn, ∼ 255 cm, LAI ∼ 3.6–2.7		Wheat, ∼ 10 cm, LAI ∼ 0.4		Wheat, ∼ 30–35 cm, LAI ∼ 1.8–3.6	
		Range	Mean (median)	Range	Mean (median)	Range	Mean (median)	Range	Mean (median)	Range	Mean (median)
Air temperature	°C	9.7–30.1	20.4 (20.0)	13.4–38.1	26.9 (26.4)	8.5–33.7	21.1 (21.3)	−13.1–6.6	−2.2 (−2.3)	0.0–22.8	9.8 (9.8)
Soil temperature	°C	14.7–26.3	19.9 (19.4)	18.9–32.9	26.6 (26.7)	17.5–26.7	22.0 (21.8)	−6.6–0.0	−1.5 (−0.8)	1.5–22.3	10.9 (10.4)
Air humidity	%	1.7–99.7	84.3 (90.7)	18.1–99.3	59.1 (59.9)	33.7–99.8	85.2 (92.4)	52.7–99.8	90.7 (95.1)	34.3–100	73.0 (74.5)
Global radiation	$W\,m^{-2}$	0.6–1065.6	249.7 (54.4)	0.6–956.9	206.8 (45.6)	0.6–1010.6	176.2 (11.9)	0.6–428.1	57.1 (0.6)	0.6–890.6	158.4 (7.5)
Leaf wetness	%	3.5–100.0	42.8 (19.4)	2.4–100.0	19.9 (5.3)	5.9–100.0	59.4 (91.9)	5.9–100.0	89.5 (100.0)	2.4–100	37.0 (8.2)
Precipitation	mm	–	0.2	–	1.2	–	13.6	–	4.0	–	8.0
PAR photon flux	µE	1.2–1956.2	449.6 (91.6)	1.2–1826.2	414.0 (106.2)	1.2 -2021.2	350.3 (26.2)	1.2–778.7	104.5 (1.2)	1.2–1621	298 (13.7)
Soil water content	(% vol)	10.4–21.6	14.6 (14.0)	5.5–36.6	11.1 (8.1)	28.0 -30.5	29.0 (28.9)	4.6–14.6	6.4 (6.1)	5.3–8.8[b]	6.3 (6.1)[b]
Wind speed	$m\,s^{-1}$	0.01 −4.08	1.32 (1.22)	0.01–7.24	2.00 (1.74)	0–6.08	1.00 (0.86)	0.01 −7.61	2.02 (1.67)	0.00–8.91	2.74 (2.60)
Friction velocity	$m\,s^{-1}$	0.01–0.54	0.16 (0.15)	0.01–0.71	0.18 (0.17)	0–0.61	0.13 (0.10)	0.01–0.75	0.15 (0.12)	0.00–1.59	0.23 (0.19)
σ_w	$m\,s^{-1}$	0.01–0.67	0.19 (0.19)	0.01–0.79	0.23 (0.23)	0.01–0.63	0.14 (0.12)	0.02–0.62	0.21 (0.19)	0.01–0.88	0.29 (0.27)
Bulk canopy conductance[a]	$cm\,s^{-1}$	0–9.7	2.1(1.8)	0–2.3	0.5 (0.4)	0–8.9	2.1 (1.9)	–	–	0–9.3	1.9 (1.6)
CO_2 flux	$\mu mol\ m^{-2}s^{-1}$	−43.4–13.0	−7.7 (−1.7)	−12.5–9.4	−0.7 (0.7)	−45.3–10.9	−6.2 (−1.1)	−5.7–2.8	−0.4 (−0.1)	−40.3–11.1	−5.3 (0.1)
Latent heat flux	$W\,m^{-2}$	−211.6–551.4	119.5 (36.1)	−41.4–381.3	31.0 (17.2)	−225.8–385.7	62.3 (18.5)	−179.6–268.2	6.1 (4.3)	−180.7–363.5	66.2 (36.1)
Sensible heat flux	$W\,m^{-2}$	−139.8–144.1	−4.4 (−3.8)	−93.1–343.6	59.3 (2.7)	−111.8–216.7	13.3 (−0.4)	−116.1–178.3	1.7 (−0.2)	−243.9–167.6	11.6 (−2.9)
Ambient air Hg^0 conc.	$ng\,m^{-3}$	2.22–12.57	5.19 (4.94)	1.77–10.09	3.90 (3.59)	1.87–10.57	3.42 (3.31)	2.71–13.02	6.22 (6.24)	1.21–7.28	3.72 (3.39)
Above-canopy Hg^0 flux	$ng\,m^{-2}h^{-1}$	−888.7–927.8	26.7 (13.4)	−491.8–467.6	16.5 (10.8)	−794.5–420.1	−11.8 (−6.1)	−1051.5–508.9	−11.6 (−6.7)	−926.6–483.5	17.3 (12.2)
Hg^0deposition velocity	$cm\,s^{-1}$	−2.06–1.82	−0.12 (−0.10)	−1.86–1.34	−0.04 (−0.02)	−1.19–1.50	0.10 (0.07)	−2.95–1.99	0.01 (0.04)	−2.03–1.88	−0.19 (−0.12)
Hg^0 flux data coverage	%	–	74.0	–	82.2	–	86.1	–	83.0	–	51.3
Data with developed turbulence[c]	%	–	68.9	–	75.2	–	67.7	–	70.9	–	68.0
Hg^0flux data < MDL	%	–	54	–	61	–	57	–	59	–	64
Hg^0 flux uncertainty	%	–	(32)	–	(28)	–	(36)	–	(35)	–	(29)

[a] Data for daytime when global radiation > 100 $W\,m^{-2}$.
[b] Data cover only the initial part of the campaign.
[c] Flux data associated with turbulence quality classes 0 and 1.

for THg content. Event-based Hg wet deposition and precipitation amounts were measured at an adjacent site ~ 400 m N of the field site investigated. Methodological details concerning collection and Hg analysis of foliage and precipitation samples have been described elsewhere (Zhou et al., 2013).

2.4 Post-processing, correction methods and quality assessment of flux data

The 10 Hz EC flux raw data were post-processed and quality-controlled using the open-source EddyPro 5.0 flux analysis software package (LI-COR Biosciences Inc.). A series of standard data corrections were implemented as described in Zhu et al. (2015a). Tests were applied on all 20 min fast time series raw data to qualitatively assess turbulence for the assumptions required (steady-state conditions and the fulfillment of similarity conditions) for applying MM (e.g., the EC and REA methods). Following the basic system of Mauder and Foken (2004), the resulting flux was marked with a quality flag (either 0, 1 or 2, denoting high, moderate and low quality, respectively).

The REA system enabled a mode (reference sampling) during which air is sampled synchronously with both conditional inlets (with the dynamic deadband as a threshold). Regularly during the field campaigns (every 72 h), the REA system was operated in reference sampling mode to correct for minor bias between the conditional channels in Eq. (1) following Sommar et al. (2013b).

In turn, the relative uncertainty in the REA flux ($\sigma_{F^{\mathrm{REA}}}/F^{\mathrm{REA}}$) was quantified following Kramm et al. (1999):

$$\sigma_{F^{\mathrm{REA}}}/F^{\mathrm{REA}} = \pm\sqrt{\left(\sigma_{H^{\mathrm{EC}}}/H^{\mathrm{EC}}\right)^2 + \left(\sigma_{\Delta C_{\mathrm{REA}}/\Delta C_{\mathrm{REA}}}\right)^2 + 2\cdot\left(\sigma_{\Delta T_{\mathrm{s,\,REA}}}/\Delta T_{\mathrm{s,\,REA}}\right)^2}. \quad (5)$$

The procedures we deployed to assess uncertainty in the individual terms are described in Zhu et al. (2015b). As the sampled air was not dried, derived F^{REA} was corrected for variations in the water vapor content of the air following Lee (2000).

3 Results

3.1 Flux data coverage, detection limit and uncertainty level

Five separate flux measurement campaigns were conducted over the period May 2012 to April 2013. The time and duration of the campaigns are listed in Table 1, which also include the flux data coverage for the individual sampling periods. The total flux data coverage across the five campaigns was ~ 73 %. Gaps in the measurements mainly resulted from power failures, calibration/reference sampling periods and instrumentation failures. Precipitation events leading to malfunction of the sonic anemometer contributed ~ 15 % of the missing data. Extreme imbalances in REA updraft and downdraft sampling volumes on an undiluted basis could prevail periodically during very calm wind conditions. This translates into sub-optimal Hg mass loadings for analysis per sample concerning the channel associated with small volumes, which potentially yield a biased determination of ΔC_{REA} (Zhu et al., 2015b). Data from 20 min periods were not further processed when one of the REA channels was open for sampling less than 10 % of the total time, which accounted for ~ 12 % of the missing data. Based on the quality flag of H^{EC} data, the percentage of flux data linked with moderate to high quality turbulence during a campaign is given in Table 1. Overall, ~ 70 % of flux data belong to this category.

The precision of the REA system to resolve concentration differences (ΔC_{REA}) under field conditions was derived from periods of reference sampling and based on the standard deviation of the residuals ($\sigma_{\Delta C_{\mathrm{REA}}}$) from orthogonal linear regression fitting of the conditional sampling channel reference concentrations $C^{\uparrow}_{\mathrm{ref}}$ vs. $C^{\downarrow}_{\mathrm{ref}}$ (Zhu et al., 2015b). The ambient air Hg^0 concentration (C) dependent relationship ($\sigma_{\Delta C_{\mathrm{REA}}} = 0.057 + 0.016\cdot C, \mathrm{ng\,m^{-3}}$) obtained from fitting data from all reference periods ($n = 921$) was used to predict the method detection limit (MDL) for each flux observation. Using this criterion, the proportion of Hg^0 flux data above the MDL was calculated for each campaign and listed in Table 1. Fifty-seven percent of the Hg^0 flux measurements were above the MDL. For data integration, however, we choose to use the complete data set since average fluxes may otherwise be overestimated. The median of relative uncertainty in individual 20 min Hg^0 fluxes (derived by Eq. 5) is given for each campaign in Table 1. The medians were constant (28–35 %) across the campaigns. On a diurnal basis, relative uncertainty was generally largest during the hours after sunrise, when sensible heat fluxes shifted direction and Hg^0 concentration tended to fluctuate; cf. Zhu et al. (2015b).

3.2 Environmental conditions

Meteorological quantities measured for each campaign during the study period are summarized in Table 1. Air temperature and precipitation were within the range of mean values recorded for the site over the past decade (Bao et al., 2014). However, specifically for the Hg^0 flux measurement periods, the precipitation frequency and total depth were sparse (in total 2.7 cm) and did not notably influence soil moisture in any event. In 2012, wheat started to elongate in late March and the peak in single-sided LAI (~ 2.4) appeared in early May and then progressively declined as leaves in the underlayer turned yellow (Fig. 1). The weather during campaign 1 was generally fair and moist with stable stratification predominant during the night ($(z-d)/L = \varsigma > 0.02$, 78 % of the time; L is the Okuhkov length), while near-neutral (37 % of the time) and unstable ($\varsigma < -0.02$, 45 % of the time) conditions were frequent during daytime. The canopy was wet most nights due to dew condensation, while soil moisture

initially at $0.22\,m^3\,m^{-3}$ showed a declining trend over the period (Fig. 4a). Campaign 2 was characterized by warm (mean air temperature 27 °C) and dry weather. Unstable conditions were predominant (93 % of the time) during daytime, partially leading to free convection ($\varsigma < -1$). The senescent canopy was wet only on occasional nights and the topsoil layer was consistently dry ($0.06–0.09\,m^3\,m^{-3}$). At the end of a campaign, after wheat harvest, the field was flood irrigated (Fig. 4b). The main growing period for corn started after mid-July (DOY ~ 200) and the maximum LAI ~ 3.7 was attained during the second half of August (Fig. 1). The general meteorological condition during campaign 3 was moist with periods of cloud cover and isolated rain showers. Low wind prevailed the vast majority of the time (mean $1.0\,m\,s^{-1}$) and the canopy remained wet for protracted periods (Fig. 4c). The lower turbulent exchange during those days is represented by low values of σ_w (mean: $0.14 \pm 0.10\,m\,s^{-1}$), which has an impact on the REA flux (Eq. 1). As shown in Table 1, the mean σ_w for the period was lower than for any other campaign. Under the fully grown corn canopy, the topsoil remained moist over time ($\sim 0.28–0.31\,m^3\,m^{-3}$). Hazy days with air temperature below zero were frequent during campaign 4 over frozen ground with dormant wheat. The site was under the influence of high-pressure systems and the haze reduced surface solar radiation, thereby leading to a more stable boundary layer with near-neutral or slightly stable ($-0.02 < \varsigma < 0.20$) atmospheric stratification dominating during daytime (81 % of the time), while air was prevailingly stable during the night (79 % of the time). Snowfall occurred on 20 January and the ground was snow-covered towards the end of the period.

In 2013, the peak in the LAI for wheat was higher in magnitude (~ 3.75) and occurred already in late April. The weather conditions during campaign 5 featured moderate-to-strong wind speeds during daytime and relatively low air humidity without precipitation events. Mostly near-neutral or slightly unstable conditions were encountered during daytime (81 % of the time). During two campaigns, strong prevailing wind directions were present (campaign 2, SW; campaign 3, SSE); for another two there was a prevailing direction with a larger component of near-counter-current flow (campaign 4, SSW–N; campaign 5, SSW–NE), while the wind directions were more variable during campaign 3.

3.3 Ambient Hg^0 concentrations

The NCP is one of the most heavily impacted regions in China in terms of airborne Hg pollution and total Hg deposition fluxes (L. Wang et al., 2014). Notwithstanding that YCES is in a rural area, the surrounding NCP region has a high proportion of heavy and chemical industry clusters involving high energy consumption provided by the foremost coal-fired power plants, resulting in substantial Hg emissions into the air (Zhang et al., 2013). Hg emission sources in rural districts include domestic and field burning of crop residue (Huang et al., 2011) and illegal artisanal gold mining utilizing mercury amalgamation (AMAP/UNEP, 2013; Hall et al., 2014).

Throughout the measurement periods, concentrations of Hg^0 were significantly variable (coefficient of variation: 27–33 % for the individual campaigns). As listed in Table 1, the overall span of Hg^0 observations ranged from background values infrequently below $2\,ng\,m^{-3}$ to episodical peaks well above $10\,ng\,m^{-3}$. The overall average concentration of Hg^0 for the measurement periods was $4.3\,ng\,m^{-3}$, which exceeds the highest seasonal average ($3.5\,ng\,m^{-3}$, summer) measured at a rural site in the Beijing region (Zhang et al., 2013) and that ($2.7\,ng\,m^{-3}$, winter) measured at the tip of Shandong peninsula (Ci et al., 2011). Mean values fell between 3.4 and $5.2\,ng\,m^{-3}$ for the growing season individual campaigns (1–3, 5). Campaign 4 in January 2013 with a mean Hg^0 concentration of $6.2\,ng\,m^{-3}$ was characterized by prolonged and severe haze pollution episodes over the NCP region (L. T. Wang et al., 2014). Available data show for the Jinan municipal area, circa 50 km southeast of the site, that hourly averaged fine particulate ($PM_{2.5}$) concentrations ranged between ~ 100 and $600\,\mu g\,m^{-2}$ over the duration of campaign 4 (J. Wang et al., 2014). The Hg^0 (YCES) and $PM_{2.5}$ concentration (Jinan) time series have similar trends, implying that Hg^0 at least in part share sources with air $PM_{2.5}$ pollution. For January 2013, there is a contemporary atmospheric Hg data set collected in Qingdao (a major coastal city, ~ 340 km east) averaging $2.8 \pm 0.9\,ng\,m^{-3}$ for Hg^0 and $245 \pm 174\,pg\,m^{-3}$ for particulate-bound Hg (Zhang et al., 2014), indicating that particulate-bound Hg (PBM) makes up a substantial fraction of aerial Hg during the widespread winter haze.

All Hg^0 concentration data sets showed positive skewness and kurtosis, indicating a predominant influence of emission sources. In the panels of Fig. 2, the directionality of Hg^0 concentrations during the five campaigns was investigated by plotting pollution roses. In general, Hg^0 showed no manifest dependence on ground wind direction over the sampling periods. However, during April 2013 (Fig. 2e), the significantly lower Hg^0 concentration associated with northeasterly wind directions was tentatively identified as air masses arriving from northeastern China/Russian far east via a slower passage over the Bohai Sea (Fig. S1 in the Supplement. Diurnal Hg^0 concentration features for each of the campaigns are shown in Fig. 3. Distinct profiles, which peaked during morning/daytime and reached a minimum at dusk/nighttime, were representative for most campaigns. During these periods, Hg^0 displayed a significant negative correlation with atmospheric stability (Spearman's rank correlation, $p < 0.01$). This daily variation pattern may reflect a limited importance of local ground-based Hg^0 sources as no considerable level of Hg^0 concentrations was observed to build up within the shallow nocturnal boundary layer. First with the development of the mixed layer, concentrations increased conceivably due to mixing-in of more Hg^0-rich air from aloft.

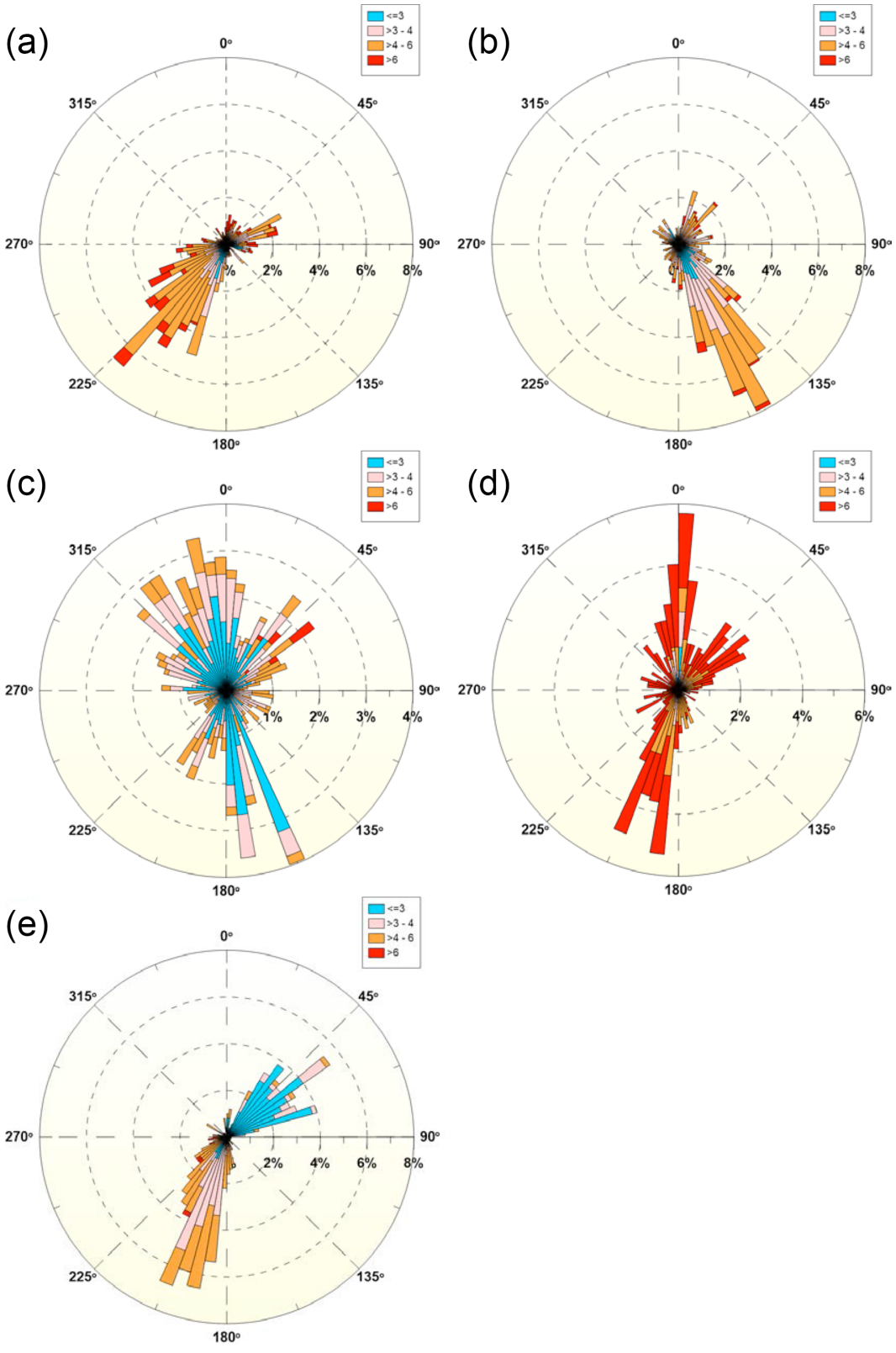

Figure 2. Polar histograms of 20 min averaged 5° per bin Hg^0 concentrations (ng m^{-3}) classified into four magnitude levels (≤ 3, >3–4, >4–6 and ≥ 6 ng m^{-3}). The letter assigned to each pollution rose refers to the campaign number in consecutive order (a = 1, b = 2, etc.).

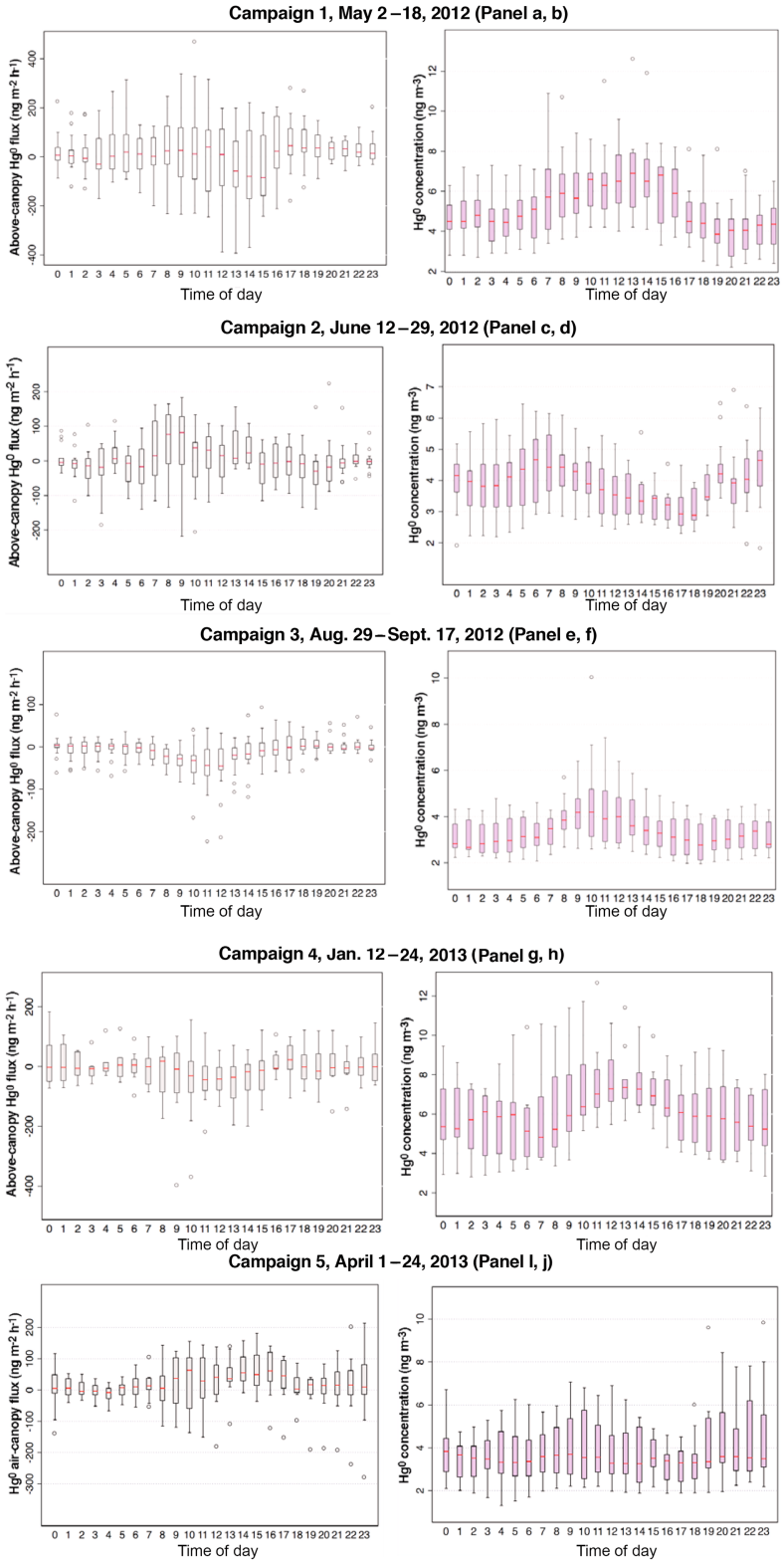

Figure 3. Diurnal variation in above-canopy Hg^0 flux (left panels) and Hg^0 concentrations during the five campaigns. Box horizontal border lines represent the 25th and 75th percentiles from bottom to top, the whiskers include the 10th and 90th percentiles, and the outliers (open circles) encompass the 5th and 95th percentiles. The solid line in the box represents the median.

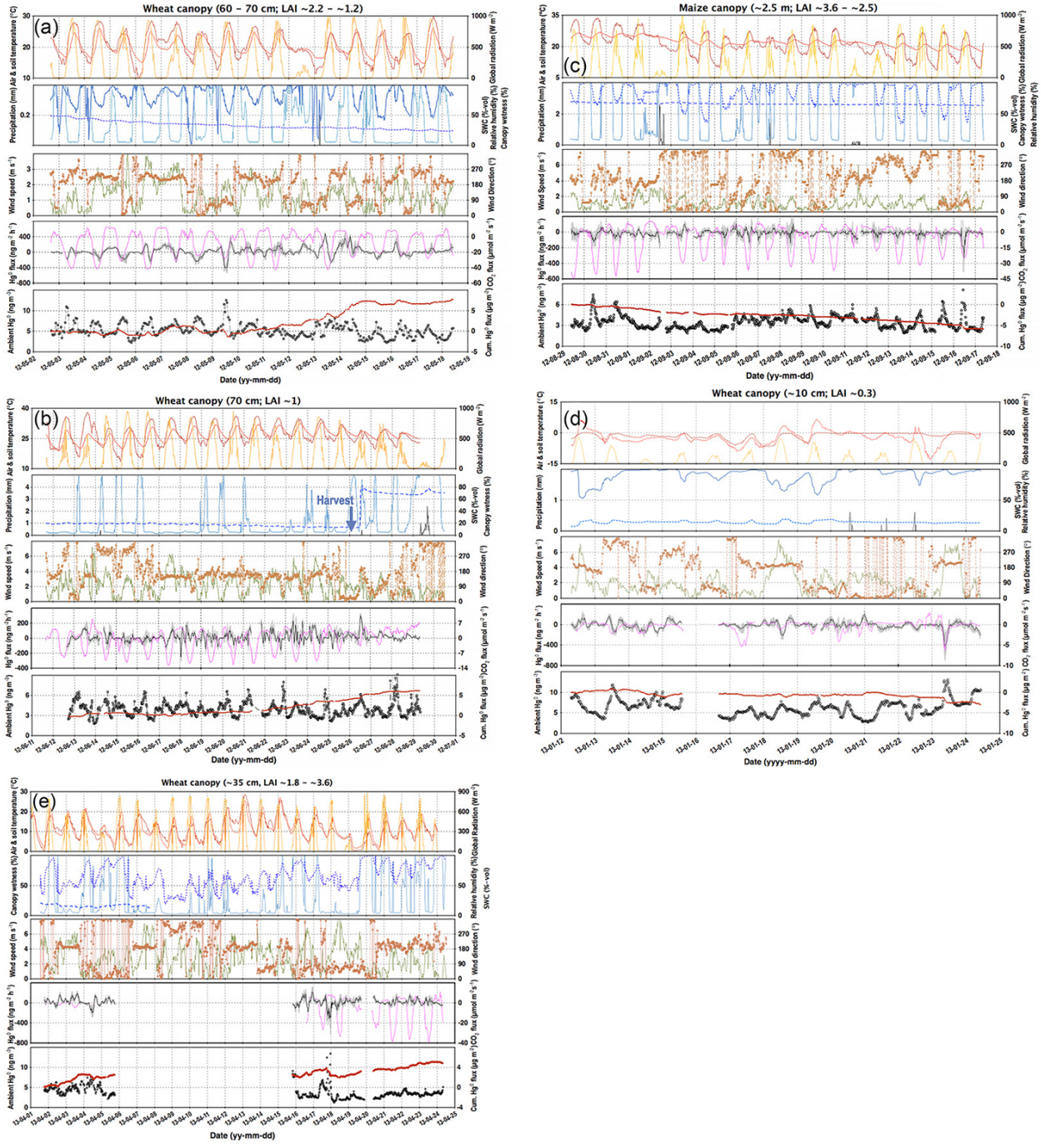

Figure 4. Time series of the selected measurement data for the individual campaigns at YCES in consecutive order **(a–e)**. Panels from the top downwards: air and below canopy surface soil temperature (°C, maroon and red solid lines, respectively) and global radiation ($W\,m^{-2}$, yellow solid line); event precipitation (mm, black solid line), relative humidity (%, blue dotted line), canopy wetness (%, grey-blue solid line) and soil water content (% volume of field capacity, blue dashed line); wind speed ($m\,s^{-1}$, olive solid line) and wind direction (°, brown open circles); smoothed Hg^0 ($ng\,m^{-2}\,h^{-1}$, black solid line) and CO_2 flux ($\mu mol\,m^{-2}\,s^{-1}$, magenta solid line); ambient air Hg^0 concentration ($ng\,m^{-3}$, grey filled circles) and cumulative Hg^0 flux ($\mu g\,m^{-2}$, maroon filled circles). Dates refer to China Standard Time (major ticks indicate midnight). Hg^0 flux data were smoothed by a nine-point moving average, where the shaded grey area represents its standard deviation. In Fig. 4b the blue arrow associated with caption "Harvest" indicates the end of the wheat harvest that started on 23 June.

Table 2. Spearman's rank-order correlation coefficients between Hg^0 flux (REA method), Hg^0 air concentration and other measured parameters. Significance levels $p < 0.01$ and $p < 0.001$ are indicated by italic and black bold-faced fonts, respectively.

Variable	2–18 May 2012		12–29 Jun 2012		29 Aug–17 Sep 2012		12–24 Jan 2013		1–24 Apr 2013	
	Ambient air Hg^0	Hg^0 flux	Ambient air Hg^0	Hg^0 flux	Ambient air Hg^0	Hg^0 flux	Ambient air Hg^0	Hg^0 flux	Ambient air Hg^0	Hg^0 flux
Air temperature	**0.15**	**−0.10**	**−0.44**	0.04	**0.30**	**−0.14**	**0.29**	0.05	**0.39**	0.06
Soil temperature	−0.01	**−0.13**	**−0.42**	0.01	**0.14**	**−0.22**	**0.17**	0.03	**0.21**	*0.11*
Air humidity	**0.12**	**0.19**	**0.19**	−0.05	−0.01	**0.17**	−0.01	*−0.10*	−0.00	**−0.21**
Global radiation	**0.20**	**−0.20**	**−0.18**	0.07	**0.28**	**−0.29**	**0.38**	**−0.16**	0.04	**0.19**
Leaf wetness	0.07	**0.14**	**0.28**	0.01	**−0.10**	**0.18**	**−0.14**	0.05	**0.18**	**−0.23**
PAR photon flux	**0.21**	**−0.19**	**−0.19**	0.07	**0.25**	**−0.27**	**0.38**	**−0.17**	0.04	**0.19**
Soil water content	**0.24**	**−0.19**	−0.01	−0.07	*−0.08*	0.03	**0.21**	0.01	–	–
Wind speed	**0.28**	**0.14**	**−0.23**	**0.35**	**0.17**	**−0.26**	*0.09*	**0.25**	**−0.26**	**0.37**
Friction velocity	**0.37**	*0.08*	**−0.21**	**0.29**	**0.22**	**−0.28**	0.08	**0.26**	**−0.37**	**0.13**
Bulk canopy conductance	**0.28**[a]	0.08[a]	−0.12[a]	**0.23**[a]	*0.19*[a]	−0.14[a]	–	–	**−0.23**[a]	**−0.33**[a]
CO_2 flux	**−0.25**	**0.25**	−0.02	0.01	**−0.19**	**0.23**	**−0.23**	**0.17**	−0.09	*−0.12*
Latent heat flux	**0.21**	**−0.14**	**−0.28**	0.00	**0.21**	**−0.25**	**0.15**	0.07	**−0.14**	0.07
Sensible heat flux	*0.09*	**−0.24**	−0.08	*−0.10*	**0.28**	**−0.12**	**0.42**	**−0.29**	**0.19**	0.05
Ambient air Hg^0	–	**−0.30**	–	−0.03	–	**−0.26**	–	**−0.35**	–	−0.07
Hg^0 flux	**−0.30**	–	−0.03	–	**−0.26**	–	**−0.35**	–	−0.07	–

[a] Data for daytime when global radiation $> 100\ W\,m^{-2}$.

This is indicative of the intensity of regional Hg emission sources. In contrast, during the June campaign, episodes of elevated Hg^0 values occurred during series of nights associated with slightly stable conditions and low wind speeds ($< 3\ m\,s^{-1}$), but without a discernible dependence of wind direction (Fig. 4b). All of this suggests that the peaks derive from nocturnal in-field burning of crop residue occurring in the surrounding countryside during the harvest season (Huang et al., 2011).

3.4 Cropland–atmosphere exchange of Hg^0 and CO_2

In order to research the Hg^0 exchange between a cropland and the atmosphere, it is necessary to understand the seasonal variation in key environmental factors. For example, measured CO_2 net exchange provided valuable information about crop productivity and farmland ecosystem respiration over time. In Table 1, a statistical summary of Hg^0 and CO_2 net fluxes is given for the five sampling periods. Since both the distribution of Hg^0 fluxes and air concentrations deviated for several of the campaigns significantly from normality (Shapiro–Wilk test, $p < 0.001$), the median is supplied in Table 1 as an estimator of central tendency. Moreover, the statistical dependence between variables was assessed by non-parametric tests (Spearman's rank correlation, Table 2). Due to a large spread in Hg^0 flux data, numerical smoothing was in this study performed on all data sets using a nine-point moving average (which corresponds to an interval of 3 h) to reduce the variability and therefore allow for a better visual interpretation of diurnal variations (Cobos et al., 2002; Fritsche et al., 2008c). The associated time series of smoothed Hg^0 and CO_2 fluxes are displayed in the composite Fig. 4. However, since the smoothing procedure introduces data manipulation, smoothed data are not used in any statistical treatments (such as correlation analysis, Table 2) or in the calculation of cumulative fluxes (shown in Figs. 4 and 8).

3.4.1 Average and ranges of fluxes for the different measurement periods

Previous studies of the wheat–corn rotation farmland at YCES evinced it to be a significant sink of atmospheric CO_2 during the main growing seasons of winter wheat and corn (e.g., Li et al., 2006; Tong et al., 2014), which for our study overlap with campaigns 1 (May) and 3 (August–September) and the end part of campaign 5 (late April). Using the EC technique, mean CO_2 uptakes of 7.7, 6.2 and 6.7 $\mu mol\,m^{-2}\ s^{-1}$ were determined for each of these sampling periods (cf. Fig. 4a, c and e). For the senescent wheat (campaign 2), CO_2 uptake declined rapidly and in turn ecosystem CO_2 respiration progressively gained more importance during daytime (with increased maximum temperatures), resulting in a mean CO_2 net exchange slightly below zero ($-0.7\ \mu mol\,m^{-2}\,s^{-1}$). The average Hg^0 above-canopy net flux was positive for the main growing season of winter wheat until harvest (April: 17.3; May: 26.7; and June: $16.5\ ng\,m^{-2}\,h^{-1}$), while slightly dry deposition of Hg^0 predominated over the field, with a fully developed corn canopy (August–September, mean flux $-11.8\ ng\,m^{-2}\,h^{-1}$). DFC measurements underneath the developed canopies show sig-

nificant Hg^0 soil emissions during daytime (Fig. 5). In more detail, mean air–soil Hg^0 fluxes were more strongly evasive under the wheat canopy (May: 39.9; June: 31.5 ng m^{-2} h^{-1}) than under the denser corn canopy (August–September: 10.8 ng m^{-2} h^{-1}). Sampling periods conducted over wheat in early growing stages were characterized by near-zero mean CO_2 net flux (November: 0.5; January: −0.4; and early April: −0.7 µmol m^{-2} s^{-1}). As reported in Zhu et al. (2015a), collocated MM and chamber flux measurement systems gauged unanimously positive net Hg^0 flux (mean range: 2.2–7.6 ng m^{-2} h^{-1}) over the field during November. Hg^0 fluxes during early April were also predominantly positive (mean: 19.5 ng m^{-2} h^{-1}), while the cumulative Hg^0 flux was negative (mean: −11.6 ng m^{-2} h^{-1}) for the winter period (campaign 4) involving prolonged and severe haze air pollution episodes.

Irrespective of sampling period, extreme values in net Hg^0 exchange (Table 1) were observed primarily during and after episodes when air with highly elevated Hg^0 concentration advected over the fetch. Although highly dynamic, vertical fluxes of Hg^0 were on average substantially negative during such an event (cf. Fig. 4). On several occasions, the REA system gauged significant emission fluxes during the immediate period following a major Hg^0 dry deposition event. This temporal development also seen in other studies (Bash and Miller, 2007; Cobbett and Van Heyst, 2007) demonstrates the potential of deposited Hg^0 to be promptly recycled to the atmosphere.

During most of the sampling campaigns, above-canopy Hg^0 flux followed a discernible diurnal pattern, with the absolute magnitude of the flux being largest during daytime periods and generally small at night (Fig. 3). However, the cycle of prevailing developed and weak atmospheric turbulence during day and night, respectively, was periodically disrupted by windy conditions extending into dark hours, facilitating turbulent exchange (mostly encountered in winter and spring campaigns; Fig. 3g and i).

3.4.2 Hg^0 flux patterns during the main growing season

Although the REA measurements during the spring and summer campaigns indicate the wheat cropland to be a continual net source of atmospheric Hg^0, the correlation (ρ, Spearman's rank-order correlation coefficient) between Hg^0 flux and other measured parameters varied significantly between the individual campaigns (Table 2). In contrast to a well-defined diurnal pattern in soil Hg^0 efflux observed over the campaigns (Fig. 5), the average profiles in above-canopy Hg^0 flux were non-uniform at the diurnal timescale. As shown in Fig. 3, Hg^0 net fluxes above wheat canopies before canopy closure (April) and during senescence (June) were positive during daytime and from sunrise to noon, respectively, while at the anthesis stage (May) composite flux data aligned to the early afternoon minimum with mean deposition. The close agreement between the chamber and micrometeorological

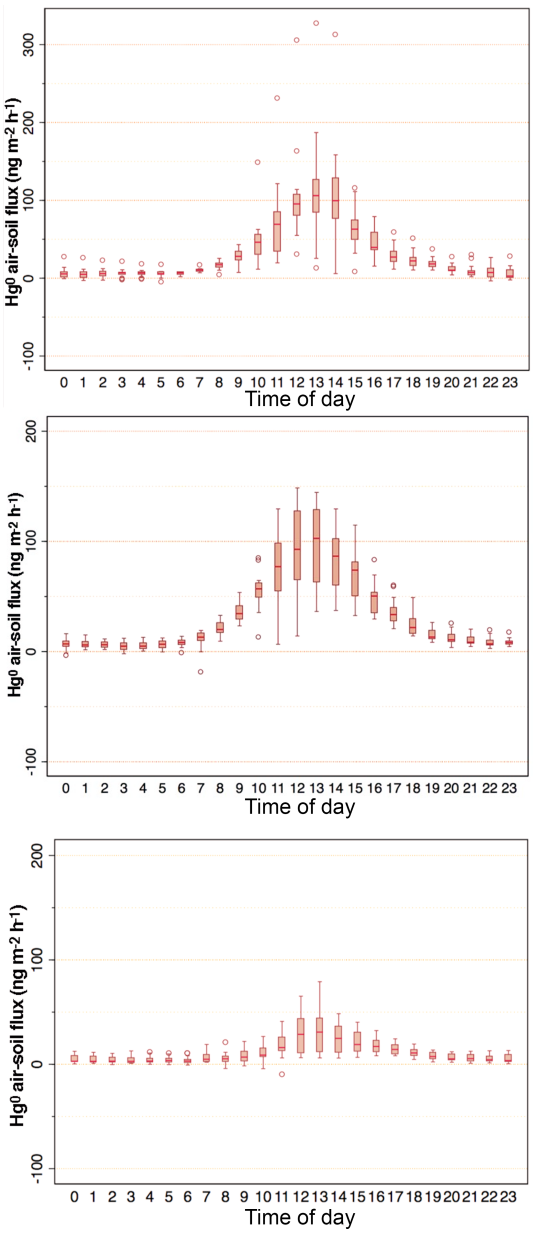

Figure 5. Diurnal variation in air–soil Hg^0 flux measured by a DFC underneath the developed canopies (upper: campaign 1; middle: 2; lower: 3): Note the divergent axis scale for the plot in the middle panel. Box horizontal border lines represent the 25th and 75th percentiles from bottom to top, the whiskers include the 10th and 90th percentiles, and the outliers (open circles) encompass the 5th and 95th percentiles. The solid line in the box represents the median.

estimates during field inter-comparison (Zhu et al., 2015a) prompted us in the present study to interpret Hg^0 in-canopy fluxes from the difference between REA and DFC observations despite the fact that the methods cover different spatial scales. For two of the campaigns (1 and 3) during the final vegetative stage of corn and wheat, ground and above-canopy Hg^0 fluxes displayed inversed daytime courses with

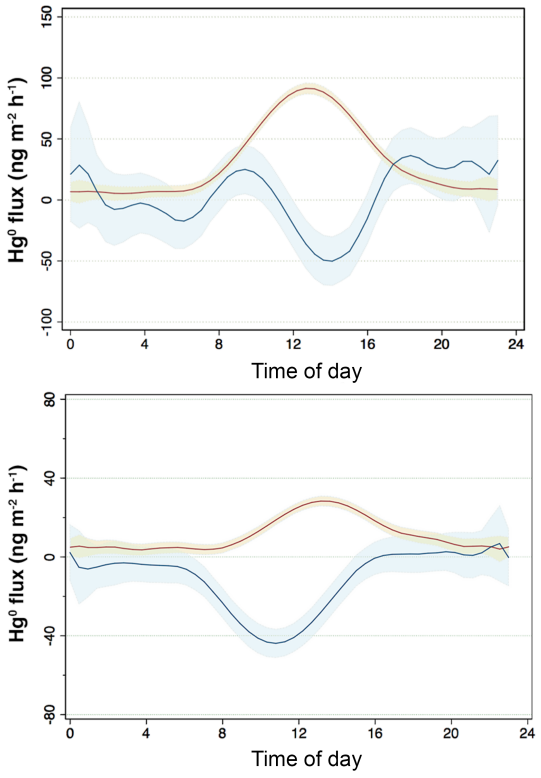

Figure 6. Local polynomial-smoothed diurnal curves of above-canopy (blue line) and ground (maroon line) Hg^0 flux during campaigns 1 (upper panel) and 3 (lower panel). Lines and envelopes depict mean and 90 % confidence intervals. Note the divergent *y* axis scales for the plots.

near mid-day maximum and minimum, respectively (Fig. 6). These data supported the hypothesis that the active growing and developed cereal canopies acted as a daytime sink of Hg^0 and at least in part were able to offset the concurrent emission from ground surfaces. During these periods, above-canopy Hg^0 flux was negatively correlated with air Hg^0 concentration and positively correlated with CO_2 flux (Table 2). To examine temporal variability of fluxes in more detail, specific observations for campaigns 1 and 3 are presented in succession below.

During daytime for a series of days with significant CO_2 uptake (4–9 May), Hg^0 dry deposition was predominant (Fig. 4a). From the middle of the campaign and onwards, periods of above-canopy Hg^0 emission become more frequent than deposition during daytime. Such a trend in above-canopy Hg^0 flux is not reflected in ground Hg^0 flux and may therefore be related to in-canopy Hg^0 source/sink characteristics. During the May period, the mean Hg^0 net fluxes were negative for the hours coincident with the diurnal maximum in Hg^0 concentration (Fig. 3a, b). Given the indication for Hg^0 uptake by the canopy when ambient concentrations were elevated, lower Hg^0 concentrations during the second phase of the period together with an expected decline in Hg^0 uptake with growth progression (Du and Fang, 1983) may explain the result. The principal diel period of Hg^0 deposition did not concur with the peak canopy conductance during morning hours, suggesting that foliar uptake of Hg^0 is not limited by periods of ample stomatal conductance. Instead, maximum mean Hg^0 deposition during campaign 1 appeared in the early afternoon, which is in concert with that of O_3 observed in a contemporary study of wheat at YCES (Zhu et al., 2015). Daytime deposition of Hg^0 was also gauged over fully leafed graminaceous plant canopies by Lee et al. (2000) and Fritsche et al. (2008c) and attributed to plant biological activities such as photosynthesis. Since net Hg^0 fluxes were bi-directional with atmospheric Hg^0 concentrations appearing to play a significant role in controlling flux, the response may be interpreted with the concept of an Hg^0 canopy compensation point (Bash and Miller, 2009; Ericksen and Gustin, 2004; Hanson et al., 1995; Poissant et al., 2008). The apparent compensation point calculated from linear regression ($r = -0.32,\ p < 0.001$) was at $\sim 5.3\,\mathrm{ng\,m^{-3}}$ for May. However, it is clear that the parameter is a composite term that is influenced by component sources/sinks within the canopy as well as at the ground (Wright and Zhang, 2015). In particular, air–soil Hg^0 flux observations were overall not linked to compensation point behavior ($r = 0.07,\ p = 0.22$), but were largely governed by the effect of global radiation and soil temperature (explaining 68.3 % of the variance in the total data; stepwise multivariate regression).

Without much day-to-day variation, Hg^0 dry deposition occurred during daytime over the whole of campaign 3 (Fig. 4c). At the diurnal timescale, Hg^0 flux shows a shallow minimum ($\sim -40\,\mathrm{ng\,m^{-2}\,h^{-1}}$) over corn just before noontime, coinciding with the peak in atmospheric Hg^0 concentration (Fig. 3e, f). Under the dense corn canopy structure the magnitude of daytime Hg^0 efflux from soil was on average a factor of ~ 3 lower compared to that within the wheat canopy (Fig. 5) and may be attributed to a combination of lower light transmission to the ground and profoundly dampened diurnal courses in surface soil temperature (cf. Fig. 4). In addition, the entirely moist surface soil may restrain Hg^0 evasion by reducing its mobility through the soil profile (Schlüter, 2000). The divergence in the dynamic scale of the diurnal Hg^0 fluxes observed at each vertical level (Fig. 6) indicates that corn with a higher above-ground biomass is a weaker Hg^0 sink (per leaf area) than wheat, as has previously been inferred from controlled experiments (Browne and Fang, 1983; Niu et al., 2011). Hg^0 uptake in cereals is plausibly associated with the enzymatic conversion of Hg^0 to Hg^{II} species within the foliar cavity (Du and Fang, 1983). Transient Hg^0 foliar uptake during campaigns 1 and 3 (encompassing similar meteorological conditions, Table 1) as calculated from the integrated imbalances between ground and above-canopy fluxes during daytime was at 0.17 ± 0.08 and $0.46 \pm 0.32\,\mathrm{\mu g\,m^{-2}}$ leaf area $\mathrm{day^{-1}}$, respectively. The apparent canopy compensation point of $\sim 3.6\,\mathrm{ng\,m^{-3}}$ is lower than that derived for the wheat

during campaign 1. The discrepancy may in part be explained by the greater positive responses in Hg^0 uptake to both light and temperature for wheat (C_3 plant) compared to corn (C_4 plant) reported by Du and Fang (1982). Essentially, above-canopy Hg^0 dry deposition during campaign 1 was confined to the mid-day, which was characterized by elevated Hg^0 in addition to high temperatures and irradiance. Individually all these parameters have been reported to significantly promote Hg^0 uptake by wheat (Du and Fang, 1982) and in close association their combined effect appear required to offset the substantial ground emission of Hg^0.

The dynamics of Hg^0 flux over wheat during the April and June campaigns with net Hg^0 emission prevailing during daytime and small nocturnal median fluxes suggests a limited capacity of the canopy to recapture Hg^0 efflux from the ground. Being a C_3 plant, the foliar Hg^0 uptake is susceptible to light and temperature conditions (Du and Fang, 1982). Under sub-optimal conditions with a low leaf temperature present in April (mean air temperature 9.8 °C), resistances are accordingly increased and rates of Hg^0 net uptake by wheat foliage are presumably lower. Over the senescent canopy, Hg^0 flux showed frequently a profound short-term temporal variability overlaid on a trend towards higher emission rates (Fig. 4b). The changing physiological properties of wheat occurring after the onset of senescence (Grossman-Clarke et al., 1999) together with crop water stress might account for the disparity between early phase May and June daytime Hg^0 canopy-scale fluxes. A prominent feature of the average diurnal pattern of the latter fluxes is the more largely Hg^0 net emission during the early morning (Fig. 3c). The temporary low Hg^0 ground evasion (mean: $9.9 \pm 25.0\,\mathrm{ng\,m^{-2}\,h^{-1}}$) indicates that the episodical Hg^0 emissions stem from above the ground (cf. Fig. 5b). Owing to the dry conditions, we may exclude the possibility of Hg^0 deriving from evaporation of dew-wetted foliar surfaces. It is more likely that the morning peak in Hg^0 flux results from canopy release of Hg^0 (following the timing of maximum values of g_c, and there is an overall positive correlation between flux and g_c, $\rho = 0.23$, $p < 0.001$) and venting of the canopy by increasing wind speeds. For wheat, there is observational evidence for transpiration flow transport of Hg^{II} species (Khozhina et al., 2001), which may become chemically reduced when reaching mesophyll through electron transfer schemes from the anti-oxidative defense system via ascorbate and potentially emitted as Hg^0 (Battke et al., 2005). In association with rapid decline in canopy transpiration (Table 1) and enzymatic-mediated Hg^0 oxidation in mature wheat (Du and Fang, 1983), our result suggests a capacitance of Hg^0 storage within the substomatal cavity that is released when the stomata are open. The fact that the morning peak in Hg^0 emission occurs, albeit with an elevated Hg^0 concentration in the air, gives more credibility to this hypothesis.

3.4.3 Hg^0 flux patterns during the non-growing season

For the periods with a near-zero CO_2 net flux indicative of non-significant plant growth, there is a marked difference between overall Hg^0 net emission occurring during late fall and early spring and net deposition during mid-winter (Tukey–Kramer test, $p < 0.01$). The experimental field with emerging wheat was relatively dry during these sampling periods (soil moisture content at 5 cm depth of 0.06–0.17 $\mathrm{m^3\,m^{-3}}$). Without a significant canopy cover, the farmland–atmosphere Hg^0 net exchange gauged during these periods would essentially derive from soil fluxes. In correspondence to air–soil Hg^0 fluxes measured within the developed canopies during warmer seasons (Fig. 5), field-scale Hg^0 fluxes were during November associated with an average diurnal profile featuring maximum emission near midday ($\sim 40\,\mathrm{ng\,m^{-2}\,h^{-1}}$; Fig. 9 in Zhu et al., 2015a). The higher mean Hg^0 fluxes observed during early April compared to November (Sect. 3.4.1) may in part be linked to warming soil temperatures during the former period (mean: 10.9 vs. 5.3 °C) given the similar level of surface soil moisture. Numerous studies have shown that surface soil temperature has a strong influence on relatively dry soil Hg^0 efflux due to its role in enhancing volatilization (Carpi and Lindberg, 1997; Gustin et al., 1997; Poissant et al., 2004; Xiao et al., 1991). In the current study, Hg^0 dry deposition occurred more frequently than emission at daytime (Fig. 3g) during the winter period with sub-zero ground temperatures (Fig. 4d). In contrast to the late fall and early spring period, Hg^0 fluxes were in winter significantly negatively correlated with Hg^0 concentration ($\rho = -0.35$, $p < 0.001$). A better part of the cumulative Hg^0 flux occurred in a few distinct periods (13–15 and 22–24 January, Fig. 4d), whereas for the remainder there was small day-to-day variation. These periods were characterized by more extreme values in Hg^0 and $PM_{2.5}$ air pollution (Sect. 3.3). In addition, snowfall samples collected had elevated Hg concentrations (Sect. 3.5), suggesting enrichment by scavenging of Hg bound to aerosols. It should be noted that Hg^0 fluxes reported here for winter could represent extremes rather than average seasonal conditions. As can be seen in Fig. 4d, events of substantial Hg^0 dry deposition were in general followed by a period of net emission, suggesting frozen surfaces to be a transient sink for atmospheric Hg^0. Cobbett and Van Heyst (2007) also found that elevated concentrations of Hg^0 ($> 10\,\mathrm{ng\,m^{-3}}$) resulted in highly dynamic net Hg^0 fluxes over agricultural soil below 0 °C with dry deposition shifting to emission, whereas net exchange was concomitantly low under ambient conditions.

3.4.4 Flux responses to abrupt changes in environmental conditions

Hg^0 flux data were examined for a discernible response to abrupt changes in environmental conditions due to agricultural management operations (e.g., tilling and irrigation) and

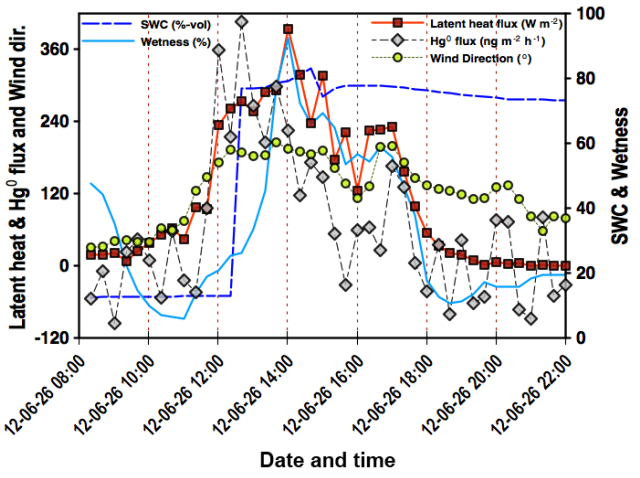

Figure 7. Time series of latent heat flux (W m^{-2}, red filled squares), Hg^0 flux (grey filled diamonds), wind direction (°, yellow filled circles), soil water content (% of field capacity, dashed dark blue line) and leaf wetness (%, light blue solid line) measured during and after field irrigation (26 June).

precipitation as such events have previously been linked to increases in Hg^0 emissions from soils (Bash and Miller, 2007; Baya and Van Heyst, 2010; Gillis and Miller, 2000; Lindberg et al., 1999). In June 2012, while the topsoil was substantially dry ($\sim 0.06\,m^3\,m^{-3}$), wheat harvest (the fields making up our primary fetch) started on 23 June and was completed the next day. The harvesting had no discernible boosting effect on Hg^0 concentration in the air, while Hg^0 air–surface exchange showed significant bi-directional fluctuations during this period, yielding a surplus of Hg^0 emission (Fig. 4b). In turn, field flood irrigation was conducted on 26 June starting from the southern end of the field south of the eddy tower (distance ~ 130 m). The flooding of the southern field was completed soon after noon (indicated by the ramp in soil moisture measured near the flux tower, Fig. 7). During most of this irrigation period the REA flux footprint falls outside the primary area. However, as wind gradually turned towards southerlies (and increased from ~ 2 to $\sim 4\,m\,s^{-1}$), the integrated flux signal derived increasingly from wetted field surfaces, with good representativeness commencing at noon and following for a few hours (90 % isopleth footprints predicted at 107 ± 43 m during this period; concerning the models employed for this purpose, cf. Sommar et al., 2013b). As seen in Fig. 7, Hg^0 and water vapor fluxes jointly show enhancement after the wind transition, indicating that volatilization of Hg^0 from soils occurred in response to field irrigation. After initial spike-like features ($> 300\,ng\,m^{-2}\,h^{-1}$), there is a decline in Hg^0 flux over the time the irrigated field was upwind of the measurement system (until $\sim$ 17:30). Similar observations have been made from field and controlled laboratory experiments, where prompt and substantial release of Hg^0 from soils has been observed following precipitation/irrigation provided the soil initially was quite dry (Bahlmann et al., 2004; Lindberg et al., 1999; Song and Van Heyst, 2005). Possible causes of the observed pattern include physical displacement of soil pore air enriched in Hg^0 and desorption of Hg^0 loosely bound onto surfaces as water percolates into the soil (Lindberg et al., 1999). Over the course of the rest of campaign 2, the magnitude and variability in Hg^0 flux were substantially lower (minor emission flux predominant) than before irrigation (Fig. 4b). In correspondence, Schroeder et al. (2005) found that persistent rain and high soil moisture contents inhibit Hg evasion from soils, which could be linked to restrictions in the replenishment of Hg^0 towards the soil surface due to low diffusivity through water-filled micropores (Schlüter, 2000). Overall, precipitation events were scarce during the flux measurement periods. During campaign 3, two substantial precipitation events occurred on 2 and 7 September (cf. Fig. 4c), but none of the events yielded any discernible enhancement in Hg^0 emission (unanimously gauged by REA and DFC). As aforementioned, surface soil was relatively moist during this period, which may have acted as a controlling factor (Song and Van Heyst, 2005).

3.5 Wet deposition Hg fluxes and mature crop foliar Hg concentrations

For the study period with a precipitation depth of 51 cm, the volume-weighted mean THg concentration in precipitation was $17.2\,ng\,L^{-1}$, corresponding to a cumulated wet deposition flux of $8.8\,\mu g\,Hg\,m^{-2}$ (Fig. 8). Maximum concentrations ($-113.3\,ng\,L^{-1}$) were detected in event precipitation during winter. However, ~ 65 % of the THg wet deposition flux for the period occurred during the summer months due to the largely asymmetric pattern in annual precipitation (cf. Fig. 8 and Table S1 in the Supplement). The large temporal variability and range of concentrations among the samples (Table S1) correspond well to observations at rural sites influenced by strong regional Hg combustion sources (Keeler et al., 2006; Schwesig and Matzner, 2000).

The THg content in mature corn and wheat foliage associated with stands of a dry leaf mass density of $\sim 0.5\,kg\,m^{-2}$ was determined to be 36.4 ± 3.1 ($n = 3$) and $122.9 \pm 13.9\,ng\,g^{-1}$ dry weight ($n = 6$), respectively. The observed foliar Hg level is comparable with the results obtained from controlled exposure of corn and wheat to elevated Hg^0 concentrations in air (Niu et al., 2011). The higher Hg accumulation in wheat compared to corn foliage aligns well with the differential Hg^0 uptake inferred from Hg^0 flux measurements (Sect. 3.4.2). Furthermore, compartmentalized Hg analysis of mature corn plants shows the Hg content increased in the order root ($5.7 \pm 1.1\,ng\,g^{-1}$, $n = 5$) < stem ($12.8 \pm 3.5\,ng\,g^{-1}$, $n = 5$) < foliage, which is indicative that vegetative uptake of airborne Hg^0 is primarily retained in cereal crop leafage. Worth noticing is also the THg content in our wheat foliage samples exceeding the maximum level

(110 ng g^{-1} dry weight) in animal feeding material (forage) issued by the European Union (EC, 2002). In addition, a survey of heavy metals in wheat and corn crops grown in the study area by Lin et al. (2010) has revealed Hg content in wheat grain at levels proximate to or prevalently exceeding the Chinese tolerance limit for food (20 ng g^{-1} dry weight).

4 Discussion

4.1 Hg^0 exchange between atmosphere and grain croplands

Measurements over the wheat–corn rotational cropland on the NCP show that each of the vegetation and soil exchange processes is important in defining net Hg^0 fluxes. The emergence of a canopy layer creates a sink for atmospheric Hg, while the canopy cover reduces the potential of underlying soil to act as an Hg^0 source. Our data also indicate that besides vegetation density (LAI) and the physical plant structure, the type of cultivated cereal crop has an effect on Hg^0 gas exchange by species-specific foliage uptake rates. Nevertheless, the chamber measurement taken here evinced that ground Hg^0 emissions within developed crop canopies are substantial in the warmer season. Regardless of growing stage, Hg^0 uptake by wheat canopies is not equal to cumulatively offsetting the Hg^0 efflux from ground surfaces (April–June mean Hg^0 net flux: 20.0 ng m^{-2} h^{-1}). Flux data available in this study over corn indicate that the fully grown, dense canopy can dominate the Hg^0 exchange process, resulting in daytime net deposition. For the early growing stages of corn not measured in this study, MM flux measurements by Cobos et al. (2002) and Baya and Van Heyst (2010) over non-contaminated soils (THg: ∼ 25 and ∼ 50 ng g^{-1}, respectively) quantified net Hg^0 emission as prevailing (mean flux: 9.7 and 15.2 ng m^{-2} h^{-1}). Considering the whole micrometeorological Hg^0 flux data set collected over the full-year 2012–2013 study period (using REA during campaigns 1–5 and MBR during IC in November, Zhu et al., 2015a) yields an overall mean Hg^0 evasion flux of 7.1 ng m^{-2} h^{-1}, accounting for nearly 5700 individual Hg^0 flux observations. Although there are substantial periods over the 2012–2013 study when flux measurements were not conducted, it appears that the wheat–corn rotational cropland investigated constitutes a net source of atmospheric Hg^0 on an annual basis. Any definite estimate of annual Hg^0 flux is however not feasible due to the large uncertainty inherent in such an attempt at extrapolation. Before a robust estimate can be constructed, other factors such as the degree of inter-annual variability must also be considered. Nevertheless, the direction and magnitude of the mean Hg^0 flux measured at our site agree well with that (6.3 ng m^{-2} h^{-1}) reported by Baya and Van Heyst (2010) for Hg^0 exchange over a soybean–corn cropland (November–April and June). For croplands, the study of Baya and Van Heyst (2010) is the only one found in the literature of temporal extent comparable with our study. Although spanning across seasons, their reported Hg^0 flux data however only marginally target seasons with substantial crop canopy closure. There are growing seasonal studies of Hg^0 net exchange over biomes predominantly vegetated by stands of non-cereal graminaceous plants. Lee et al. (2000) reported for a fetch of growing salt meadow cord grass a trend from net emission during the period before complete leaf-out (mean: 1.8 ng m^{-2} h^{-1}) to predominant dry deposition during the full foliage stage (mean: −3.3 ng m^{-2} h^{-1}). In correspondence to our study, Smith and Reinfelder (2009) observed significant daytime Hg^0 deposition over a fully grown canopy (*Phragmites australis*) coinciding with elevated ambient air concentrations.

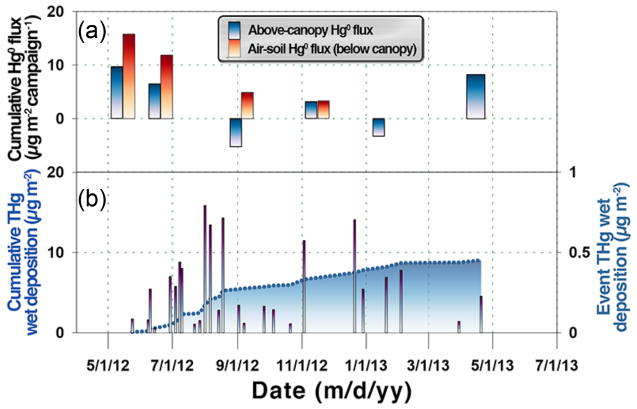

Figure 8. Time series (May 2012–May 2013) of **(a)** above-canopy (blue-shaded bars) and air–soil Hg^0 flux (red-shaded bars) cumulated for each sampling campaign and **(b)** of event-measured (shaded bars, right axis) and THg wet deposition flux cumulated over the period (dotted blue line shaded down to the abscissa, left axis).

The magnitude of average mid-day Hg^0 dry deposition over fully grown wheat and corn (Fig. 6) could be reproduced using a single-layer modeling approach (Wesely and Hicks, 1977) with a total leaf conductance parameterization to Hg^0 according to Lindberg et al. (1992) and input of average mid-day observations of conductances g_a (3.5 cm s^{-1}) and g_c (2.1 cm s^{-1}) together with C (4.1–6.6 ng m^{-3}). Associated cereal foliar Hg^0 uptake rates estimated by combined REA and DFC measurements compare in magnitude (∼ 7–19 ng m^{-2} leaf area h^{-1}) favorably with observations for aspen foliage in controlled gas-exchange systems operated at moderately elevated Hg^0 concentrations (Ericksen and Gustin, 2004; Ericksen et al., 2003). The periods with consistent daytime imbalances between above- and under-canopy flux during the early phases of campaign 1 (wheat) and campaign 3 (corn) explain up to ∼ 20 % and ∼ 50 % of the quantity of Hg accumulated by the mature foliage of wheat and corn, respectively. This indicates a relatively high contribution of the mercury load to the cereal occurring during its final vegetative stage. In many circumstances, our micrometeorological flux estimates appear better suited

to addressing the magnitude of the net cropland–atmosphere exchange and not ideal in combination with DFC for constraining vegetative Hg^0 uptake as the ground surface is the major source of Hg^0 emission. Nonetheless, controlled experiments (Niu et al., 2011) envisaged ongoing assimilation of atmospheric Hg^0 by winter wheat during its extensive period of leaf production for which we have limited REA and DFC flux data coverage.

4.2 Implications for estimation of a local Hg budget

Besides Hg^0 air–surface exchange focused on in this study, Hg input through dry deposition of other atmospheric Hg forms (gaseous oxidized mercury, GOM, and particulate-bound mercury, PBM) and bulk THg wet deposition are potentially important pathways in the local Hg cycle. Projecting the scale of THg wet deposition to Hg^0 soil emission predominant over the vast majority of the year (Fig. 8), it is unlikely that wet deposition even on a short-term basis could provide support for the magnitude of volatilization observed at YCES. Given that the top soil horizon has a uniform and low THg content, it is also unlikely that its inherent Hg pool can sustain substantial losses to the atmosphere via Hg^0 volatilization without continual replenishment. We therefore hypothesize that Hg input from a combined removal of atmospheric GOM and PBM constitutes the major deposition pathway to this site. High ratios of $PBM_{2.5}$ (Hg bound to $PM_{2.5}$) to GOM as well as of $PBM_{2.5}$ to Hg^0 are characteristic of atmospheric Hg in the NCP region (Zhang et al., 2013). In China, there is a paucity of observational Hg dry deposition studies. However, a high dry-to-wet Hg deposition ratio has been inferred from studies of Chinese forested ecosystems (Fu et al., 2015; Wang et al., 2009). Predicted total Hg deposition to the site area using simulations by the GEOS-Chem model is elevated and on the order of 80–100 $\mu g\,m^{-2}\,yr^{-1}$ (L. Wang et al., 2014), which would in theory quantitatively allow for a reasonably high Hg^0 efflux from agricultural soils in the NCP region. This presupposes that a significant portion of Hg^{II} species deposited to the ecosystem is labile towards reduction to Hg^0, which then should be extensively re-emitted back into the atmosphere. In the literature, there is support for the hypothesis that contemporary deposited Hg to a larger extent than the ambient Hg pool in terrestrial ecosystems is recycled to the atmosphere via surface photo-reduction and re-volatilization (Eckley et al., 2013; Ericksen et al., 2005; Graydon et al., 2006, 2012; Hintelmann et al., 2002). The observed abrupt pulse in Hg^0 emissions from dry soil in response to flood irrigation (Sect. 3.4.4) suggests the seasonal presence of an ample pool of Hg^0 in the upper soil horizon. Soil characteristics present at YCES such as a low level of organic matter (Edwards and Howard, 2013; Fu et al., 2012; Sigler and Lee, 2006), clayey components (Biester et al., 2002) and high alkalinity (Landa, 1978; Xin and Gustin, 2007; Yang et al., 2007) appear to facilitate Hg^0 formation, which in association with prevalent residual porosity allows for Hg^0 mobility towards the soil–air interface and losses to air. The differential magnitude of Hg^0 soil efflux measured under developed canopies with moist and dry soil, respectively, indicates that the combined level of precipitation/irrigation is one of the most important seasonal variables that control the magnitude of Hg^0 emission from the ground at the site.

5 Conclusions

In this paper, we present a broad seasonal record of Hg^0 net flux observations during 2012–2013 over a wheat–corn intercropping field located on the North China Plain. Our work appears to be the first that investigated Hg^0 gas exchange along the essential growing phases of a managed cropland from sowing to the crop maximum development. Our initial hypothesis was that the elevated atmospheric Hg^0 concentrations in the NCP region would promote depositional Hg^0 fluxes over cropland ecosystems provided with low native soil Hg content. However, during the wheat growing season covering $\sim 2/3$ of the year at the site, we observed a net Hg^0 emission prevailing during periods of active plant growth until canopy senescence (April–June mean Hg^0 net flux: $20.0\,ng\,m^{-2}\,h^{-1}$). The result can be explained by a dominance of Hg^0 emissions from ground surfaces during daytime in relation to Hg^0 uptake by overlying foliage regardless of canopy cover. In comparison to corn, the developed wheat stand provided limited canopy cover and had less effect in attenuating light and dampening the evolution of high surface soil temperatures that promoted elevated daytime soil Hg^0 efflux (daily mean maximum fluxes $> 100\,ng\,m^{-2}\,h^{-1}$) during warm seasons. Only in the fully leafed period (anthesis stage) does wheat canopy show a high capacity to recapture Hg^0 emissions from the soil during the day. Hg^0 efflux under the corn canopy near peak LAI was on average a factor of 3 lower and the temporal dynamics of net Hg^0 flux above the canopy indicated the cropland to be a weak Hg^0 sink during this period. Measurements near peak LAI of wheat and corn suggest Hg^0 exchange following the concept of a canopy compensation point (at ~ 5.3 and $\sim 3.6\,ng\,m^{-3}$, respectively). In response to agricultural management by flood irrigation, a peak of enhanced Hg^0 emission was recorded from the initially dry field as an effect of expulsion of soil gas rich in Hg^0 by infiltrating water. In conclusion, it appears that the wheat–corn rotational cropland investigated constitutes a net source of atmospheric Hg^0 on an annual basis. In addition, the practice of in-field burning of crop residue in the NCP seasonally releases a substantial amount of Hg^0 into the air from the plant material and burned soil. Due to the imbalance between THg wet deposition ($\sim 8.8\,\mu g\,m^{-2}\,yr^{-1}$) at YCES and gaseous loss by Hg^0 soil volatilization predominant over the vast majority of the year, it is suggested that dry deposition of other forms of airborne Hg (GOM and PBM) would constitute the major pathway of local Hg input. Gradual reduction of previously deposited atmospheric Hg promoted by

warming temperature and solar load may explain the summer season observation of a discernible Hg^0 soil pool. Future experimental work should besides net canopy-scale and canopy-floor Hg^0 fluxes also focus on elucidating foliage Hg exchange processes by in-canopy measurements.

The Supplement related to this article is available online at doi:10.5194/bg-13-2029-2016-supplement.

Acknowledgements. This research was supported by the State Key Laboratory of Environmental Geochemistry, the 973 program (2013CB430002), the National Science Foundation of China (41373056, 41030752) as well as the Chinese Academy of Sciences through an instrument development program (YZ200910). The technical staff of YCES is greatly appreciated for the facilities and infrastructure kindly made available to the authors.

Edited by: X. Wang

References

AMAP/UNEP: Technical Background Report for the Global Mercury Assessment 2013, Arctic Monitoring and Assessment Programme, Oslo, Norway/UNEP Chemicals Branch, Geneva, Switzerland, VI, 263 pp., 2013.

Bahlmann, E., Ebinghaus, R., and Ruck, W.: The effect of soil moisture on the emission of mercury from soils, Materials and Geoenvironment, 51, 791–794, 2004.

Bahlmann, E., Ebinghaus, R., and Ruck, W.: Development and application of a laboratory flux measurement system (LFMS) for the investigation of the kinetics of mercury emissions from soils, J. Environ. Manage., 81, 114–125, 2006.

Bao, X. Y., Wen, X. F., Sun, X. M., Zhao, F. H., and Wang, Y. Y.: Interannual variation in carbon sequestration depends mainly on the carbon uptake period in two croplands on the North China Plain, PLoS ONE, 9, e110021, doi:10.1371/journal.pone.0110021, 2014.

Bash, J. O. and Miller, D. R.: A note on elevated total gaseous mercury concentrations downwind from an agriculture field during tilling, Sci. Total Environ., 388, 379–388, 2007.

Bash, J. O. and Miller, D. R.: Growing season total gaseous mercury (TGM) flux measurements over an Acer rubrum L. stand, Atmos. Environ., 43, 5953–5961, 2009.

Battke, F., Ernst, D., and Halbach, S.: Ascorbate promotes emission of mercury vapour from plants, Plant Cell Environ., 28, 1487–1495, 2005.

Baya, A. P. and Van Heyst, B.: Assessing the trends and effects of environmental parameters on the behaviour of mercury in the lower atmosphere over cropped land over four seasons, Atmos. Chem. Phys., 10, 8617–8628, doi:10.5194/acp-10-8617-2010, 2010.

Biester, H., Müller, G., and Schöler, H. F.: Binding and mobility of mercury in soils contaminated by emissions from chlor-alkali plants, Sci. Total Environ., 284, 191–203, 2002.

Briggs, C. and Gustin, M. S.: Building upon the Conceptual Model for Soil Mercury Flux: Evidence of a Link Between Moisture Evaporation and Hg Evasion, Water Air Soil Poll., 224, 1744, doi:10.1007/s11270-013-1744-5, 2013.

Browne, C. L. and Fang, S. C.: Uptake of mercury vapor by wheat – an assimilation model, Plant Physiol., 61, 430–433, 1978.

Browne, C. L. and Fang, S. C.: Differential uptake of mercury vapor by gramineous C_3 and C_4 plants, Plant Physiol., 72, 1040–1042, 1983.

Burba, G.: Eddy covariance method for scientific, industrial, agricultural and regulatory applications: A field book on measuring ecosystem gas exchange and areal emission rates, LI-COR Biosciences, Lincoln, NE, USA, 331 pp., 2013.

Businger, J. A. and Oncley, S. P.: Flux measurement with conditional sampling, J. Atmos. Ocean. Techn., 7, 349–352, 1990.

Carpi, A. and Lindberg, S. E.: Sunlight-mediated emission of elemental mercury from soil amended with municipal sewage sludge, Environ. Sci. Technol., 31, 2085–2091, 1997.

Cavallini, A., Natali, L., Durante, M., and Maserti, B.: Mercury uptake, distribution and DNA affinity in durum wheat (Triticum durum Desf.) plants, Sci. Total Environ., 243, 119–127, 1999.

Ci, Z., Zhang, X., Wang, Z., and Niu, Z.: Atmospheric gaseous elemental mercury (GEM) over a coastal/rural site downwind of East China: Temporal variation and long-range transport, Atmos. Environ., 45, 2480–2487, 2011.

Cobbett, F. D. and Van Heyst, B. J.: Measurements of GEM fluxes and atmospheric mercury concentrations (GEM, RGM and Hg-p) from an agricultural field amended with biosolids in Southern Ont., Canada (October 2004–November 2004), Atmos. Environ., 41, 2270–2282, 2007.

Cobos, D. R., Baker, J. M., and Nater, E. A.: Conditional sampling for measuring mercury vapor fluxes, Atmos. Environ., 36, 4309–4321, 2002.

Converse, A. D., Riscassi, A. L., and Scanlon, T. M.: Seasonal variability in gaseous mercury fluxes measured in a high-elevation meadow, Atmos. Environ., 44, 2176–2185, 2010.

Cui, L., Feng, X., Lin, C.-J., Wang, X., Meng, B., Wang, X., and Wang, H.: Accumulation and translocation of ^{198}Hg in four crop species, Environ. Toxicol. Chem., 33, 334–340, 2014.

Dengel, S. and Grace, J.: Carbon dioxide exchange and canopy conductance of two coniferous forests under various sky conditions, Oecologia, 164, 797–808, 2010.

Driscoll, C. T., Mason, R. P., Chan, H. M., Jacob, D. J., and Pirrone, N.: Mercury as a global pollutant: Sources, pathways, and effects, Environ. Sci. Technol., 47, 4967–4983, 2013.

Du, S. H. and Fang, S. C.: Uptake of elemental mercury vapor by C_3 species and C_4 species, Environ. Exp. Bot., 22, 437-443, 1982.

Du, S. H. and Fang, S. C.: Catalase activity of C_3 and C_4 species and its relationship to mercury vapor uptake, Environ. Exp. Bot., 23, 347–353, 1983.

Eckley, C. S., Parsons, M. T., Mintz, R., Lapalme, M., Mazur, M., Tordon, R., Elleman, R., Graydon, J. A., Blanchard, P., and St Louis, V.: Impact of closing Canada's largest point-source of mercury emissions on local atmospheric mercury concentrations, Environ. Sci. Technol., 47, 10339–10348, 2013.

Edwards, G. C. and Howard, D. A.: Air-surface exchange measurements of gaseous elemental mercury over naturally enriched and background terrestrial landscapes in Australia, Atmos. Chem. Phys., 13, 5325–5336, doi:10.5194/acp-13-5325-2013, 2013.

Edwards, G. C., Rasmussen, P. E., Schroeder, W. H., Wallace, D. M., Halfpenny-Mitchell, L., Dias, G. M., Kemp, R. J., and

Ausma, S.: Development and evaluation of a sampling system to determine gaseous Mercury fluxes using an aerodynamic micrometeorological gradient method, J. Geophys. Res.-Atmos., 110, D10306, doi:10.1029/2004JD005187, 2005.

Engle, M. A., Gustin, M. S., Lindberg, S. E., Gertler, A. W., and Ariya, P. A.: The influence of ozone on atmospheric emissions of gaseous elemental mercury and reactive gaseous mercury from substrates, Atmos. Environ., 39, 7506–7517, 2005.

Ericksen, J., Gustin, M., Lindberg, S. E., Olund, S. D., and Krabbenhoft, D.: Assessing the Potential for Re-emission of Mercury Deposited in Precipitation from Arid Soils Using a Stable Isotope, Environ. Sci. Technol., 39, 8001–8007, 2005.

Ericksen, J. A. and Gustin, M. S.: Foliar exchange of mercury as a function of soil and air mercury concentrations, Sci. Total Environ., 324, 271–279, 2004.

Ericksen, J. A., Gustin, M. S., Schorran, D. E., Johnson, D. W., Lindberg, S. E., and Coleman, J. S.: Accumulation of atmospheric mercury in forest foliage, Atmos. Environ., 37, 1613–1622, 2003.

European Commission: Amended proposal for a Directive of the European Parliament and of the Council on undesirable substance and products in animal nutrition, Official Journal, 346e361, C096E, 27/03/2001, 2002.

Fowler, D., Pilegaard, K., Sutton, M. A., Ambus, P., Raivonen, M., Duyzer, J., Simpson, D., Fagerli, H., Fuzzi, S., Schjørring, J. K., Granier, C., Neftel, A., Isaksen, I. S. A., Laj, P., Maione, M., Monks, P. S., Burkhardt, J., Daemmgen, U., Neirynck, J., Personne, E., Wichink-Kruit, R., Butterbach-Bahl, K., Flechard, C., Tuovinen, J. P., Coyle, M., Gerosa, G., Loubet, B., Altimir, N., Grünhage, L., Ammann, C., Cieslik, S., Paoletti, E., Mikkelsen, T. N., Ro-Poulsen, H., Cellier, P., Cape, J. N., Horvath, L., Loreto, F., Niinemets, U., Palmer, P. I., Rinne, J., Misztal, P., Nemitz, E., Nilsson, D., Pryor, S., Gallagher, M. W., Vesala, T., Skiba, U., Brüggemann, N., Zechmeister-Boltenstern, S., Williams, J., O'Dowd, C., Facchini, M. C., de Leeuw, G., Flossman, A., Chaumerliac, N., and Erisman, J. W.: Atmospheric composition change: Ecosystems-Atmosphere interactions, Atmos. Environ., 43, 5193–5267, 2009.

Frescholtz, T. F., Gustin, M. S., Schorran, D. E., and Fernandez, G. C. J.: Assessing the source of mercury in foliar tissue of quaking aspen, Environ. Toxicol. Chem., 22, 2114–2119, 2003.

Fritsche, J., Obrist, D., and Alewell, C.: Evidence of microbial control of Hg^0 emissions from uncontaminated terrestrial soils, J. Plant Nutr. Soil Sc., 171, 200–209, 2008a.

Fritsche, J., Obrist, D., Zeeman, M. J., Conen, F., Eugster, W., and Alewell, C.: Elemental mercury fluxes over a sub-alpine grassland determined with two micrometeorological methods, Atmos. Environ., 42, 2922–2933, 2008b.

Fritsche, J., Wohlfahrt, G., Ammann, C., Zeeman, M., Hammerle, A., Obrist, D., and Alewell, C.: Summertime elemental mercury exchange of temperate grasslands on an ecosystem-scale, Atmos. Chem. Phys., 8, 7709–7722, doi:10.5194/acp-8-7709-2008, 2008c.

Fu, X., Feng, X., Zhang, H., Yu, B., and Chen, L.: Mercury emissions from natural surfaces highly impacted by human activities in Guangzhou province, South China, Atmos. Environ., 54, 185–193, 2012.

Fu, X. W., Feng, X. B., and Wang, S. F.: Exchange fluxes of Hg between surfaces and atmosphere in the eastern flank of Mount Gongga, Sichuan province, southwestern China, J. Geophys. Res.-Atmos., 113, D20306, doi:10.1029/2008jd009814, 2008.

Fu, X. W., Zhang, H., Yu, B., Wang, X., Lin, C.-J., and Feng, X. B.: Observations of atmospheric mercury in China: a critical review, Atmos. Chem. Phys., 15, 9455–9476, doi:10.5194/acp-15-9455-2015, 2015.

Gillis, A. A. and Miller, D. R.: Some local environmental effects on mercury emission and absorption at a soil surface, Sci. Total Environ., 260, 191–200, 2000.

Graydon, J. A., St Louis, V. L., Lindberg, S. E., Hintelmann, H., and Krabbenhoft, D. P.: Investigation of mercury exchange between forest canopy vegetation and the atmosphere using a new dynamic chamber, Environ. Sci. Technol., 40, 4680–4688, 2006.

Graydon, J. A., St Louis, V. L., Lindberg, S. E., Sandilands, K. A., Rudd, J. W. M., Kelly, C. A., Harris, R., Tate, M. T., Krabbenhoft, D. P., Emmerton, C. A., Asmath, H., and Richardson, M.: The role of terrestrial vegetation in atmospheric Hg deposition: Pools and fluxes of spike and ambient Hg from the METAALICUS experiment, Global Biogeochem. Cy., 26, GB1022, doi:10.1029/2011GB004031, 2012.

Grigal, D. F.: Mercury sequestration in forests and peatlands: A review, J. Environ. Qual., 32, 393–405, 2003.

Grossman-Clarke, S., Kimball, B. A., Hunsaker, D. J., Long, S. P., Garcia, R. L., Kartschall, T., Wall, G. W., Printer, P. J., Wechsung, F., and LaMorte, R. L.: Effects of elevated atmospheric CO_2 on canopy transpiration in senescent spring wheat, Agric. Forest Meteorol., 93, 95–109, 1999.

Gustin, M. S.: Exchange of mercury between the atmosphere and terrestrial ecosystems, in: Advances in Environmental Chemistry and Toxicology of Mercury, edited by: Cai, Y., Liu, G., and O'Driscoll, N. J., John Wiley & Sons, Hoboken, NJ, USA, 423–451, 2011.

Gustin, M. S., Taylor, G. E., and Maxey, R. A.: Effect of temperature and air movement on the flux of elemental mercury from substrate to the atmosphere, J. Geophys. Res.-Atmos., 102, 3891–3898, 1997.

Hall, C., Mao, H., Ye, Z., Talbot, R., Ding, A., Zhang, Y., Zhu, J., Wang, T., Lin, C.-J., Fu, C., and Yang, X.: Sources and dynamic processes controlling background and peak concentrations of TGM in Nanjing, China, Atmosphere, 5, 124–155, 2014.

Hanson, P. J., Lindberg, S. E., Tabberer, T. A., Owens, J. G., and Kim, K. H.: Foliar Exchange of Mercury-Vapor – Evidence for a Compensation Point, Water Air Soil Poll., 80, 373–382, 1995.

Hintelmann, H., Harris, R., Heyes, A., Hurley, J. P., Kelly, C. A., Krabbenhoft, D. P., Lindberg, S., Rudd, J. W. M., Scott, K. J., and St Louis, V. L.: Reactivity and mobility of new and old mercury deposition in a Boreal forest ecosystem during the first year of the METAALICUS study, Environ. Sci. Technol., 36, 5034–5040, 2002.

Huang, X., Li, M., Friedli, H. R., Song, Y., Chang, D., and Zhu, L.: Mercury emissions from biomass burning in China, Environ. Sci. Technol., 45, 9442–9448, 2011.

Kaimal, J. C., Wyngaard, J. C., Izumi, Y., and Coté, O. R.: Spectral characteristics of surface layer turbulence, Q. J. Roy. Meteor. Soc., 98, 563–589, 1972.

Keeler, G. J., Landis, M. S., Norris, G. A., Christianson, E. M., and Dvonch, J. T.: Sources of mercury wet deposition in Eastern Ohio, USA, Environ. Sci. Technol., 40, 5874–5881, 2006.

Khozhina E. I., Palesskii, S. V., and Saprykin, A. I.: Migration of heavy metals to the atmosphere in the process of transpiration, Atmos. Ocean. Optics, 14, 553–556, 2001 (in Russian with English summary).

Kim, K. H., Lindberg, S. E., and Meyers, T. P.: Micrometeorological measurements of mercury vapor fluxes over background forest soils in eastern Tennessee, Atmos. Environ., 29, 267–282, 1995.

Kramm, G., Beier, N., Dlugi, R., and Müller, H.: Evaluation of conditional sampling methods, Beitr. Phys. Atmos., 72, 161–172, 1999.

Landa, E. R.: Soil-water content and temperature as factors in volatile loss of applied mercury(II) from soils, Soil Sci., 126, 44–48, 1978.

Lee, X.: Water vapor density effect on measurements of trace gas mixing ratio and flux with a massflow controller, J. Geophys. Res.-Atmos., 105, 17807–17810, 2000.

Lee, X., Benoit, G., and Hu, X.: Total gaseous mercury concentration and flux over a coastal saltmarsh vegetation in Connecticut, USA, Atmos. Environ., 34, 4205–4213, 2000.

Li, J., Yu, Q., Sun, X. M., Tong, X. J., Ren, C. Y., Wang, J., Liu, E. M., Zhu, Z. L., and Yu, G. R.: Carbon dioxide exchange and the mechanism of environmental control in a farmland ecosystem in North China Plain, Sci. China Ser. D, 49, 226–240, 2006.

Li, L., Nielsen, D. C., Yu, Q., Ma, L., and Ahuja, L. R.: Evaluating the crop water stress index and its correlation with latent heat and CO_2 fluxes over winter wheat and maize in the North China Plain, Agr. Water Manage., 97, 1146–1155, 2010.

Lin, C.-J., Zhu, W., Li, X., Feng, X., Sommar, J., and Shang, L.: Novel dynamic flux chamber for measuring air-surface exchange of Hg^0 from soils, Environ. Sci. Technol., 46, 8910–8920, 2012.

Lin, J., Wang, W. Y., Li, Y. H., and Yang, L. S.: Heavy metals in soil and crops of an intensively farmed area: A case study in Yucheng City, Shandong province, China, Int. J. Environ. Res., 7, 395–412, 2010.

Lindberg, S. E., Meyers, T. P., Taylor, G. E., Turner, R. R., and Schroeder, W. H.: Atmosphere-surface exchange of mercury in a forest – Results of modeling and gradient approaches, J. Geophys. Res.-Atmos., 97, 2519–2528, 1992.

Lindberg, S. E., Zhang, H., Gustin, M., Vette, A., Marsik, F., Owens, J., Casimir, A., Ebinghaus, R., Edwards, G., Fitzgerald, C., Kemp, J., Kock, H. H., London, J., Majewski, M., Poissant, L., Pilote, M., Rasmussen, P., Schaedlich, F., Schneeberger, D., Sommar, J., Turner, R., Wallschläger, D., and Xiao, Z.: Increases in mercury emissions from desert soils in response to rainfall and irrigation, J. Geophys. Res.-Atmos., 104, 21879–21888, 1999.

Marsik, F. J., Keeler, G. J., Lindberg, S. E., and Zhang, H.: Air-surface exchange of gaseous mercury over a mixed Sawgrass-Cattail stand within the Florida Everglades, Environ. Sci. Technol., 39, 4739–4746, 2005.

Mauclair, C., Layshock, J., and Carpi, A.: Quantifying the effect of humic matter on the emission of mercury from artificial soil surfaces, Appl. Geochem., 23, 594–601, 2008.

Mauder, M. and Foken, T.: Documentation and instruction manual of EC Software Package TK2, Department of Micrometeorology, University of Bayreuth, Germany, Arbeitsergebnisse, 26, 45 pp., 2004.

Meng, B., Feng, X., Qiu, G., Cai, Y., Wang, D., Li, P., Shang, L., and Sommar, J.: Distribution patterns of inorganic mercury and methylmercury in tissues of Rice (Oryza sativa L.) plants and possible bioaccumulation pathways, J. Agr. Food Chem., 58, 4951–4958, 2010.

Millhollen, A. G., Obrist, D., and Gustin, M. S.: Mercury accumulation in grass and forb species as a function of atmospheric carbon dioxide concentrations and mercury exposures in air and soil, Chemosphere, 65, 889–897, 2006.

NBSC: China Statistical Yearbook, National Bureau of Statistics of China, Beijing, China, 1998.

Niu, Z. C., Zhang, X. S., Wang, Z. W., and Ci, Z. J.: Field controlled experiments of mercury accumulation in crops from air and soil, Environ. Pollut., 159, 2684–2689, 2011.

Niu, Z. C., Zhang, X. S., Wang, S., Zeng, M., Wang, Z. W., Zhang, Y., and Ci, Z. J.: Field controlled experiments on the physiological responses of maize (Zea mays L.) leaves to low-level air and soil mercury exposures, Environ. Sci. Pollut. R., 21, 1541–1547, 2014.

Obrist, D.: Atmospheric mercury pollution due to losses of terrestrial carbon pools?, Biogeochemistry, 85, 119–123, 2007.

Poissant, L., Pilote, M., Constant, P., Beauvais, C., Zhang, H. H., and Xu, X. H.: Mercury gas exchanges over selected bare soil and flooded sites in the bay St. Francois wetlands (Quebec, Canada), Atmos. Environ., 38, 4205–4214, 2004.

Poissant, L., Pilote, M., Yumvihoze, E., and Lean, D.: Mercury concentrations and foliage/atmosphere fluxes in a maple forest ecosystem in Québec, Canada, J. Geophys. Res.-Atmos., 113, D10307, doi:10.1029/2007JD009510, 2008.

Rinklebe, J., During, A., Overesch, M., Du Laing, G., Wennrich, R., Stärk, H. J., and Mothes, S.: Dynamics of mercury fluxes and their controlling factors in large Hg-polluted floodplain areas, Environ. Pollut., 158, 308–318, 2010.

Schlüter, K.: Review: Evaporation of mercury from soils. An integration and synthesis of current knowledge, Environ. Geol., 39, 249–271, 2000.

Schroeder, W. H., Beauchamp, S., Edwards, G., Poissant, L., Rasmussen, P., Tordon, R., Dias, G., Kemp, J., Van Heyst, B., and Banic, C. M.: Gaseous mercury emissions from natural sources in Canadian landscapes, J. Geophys. Res.-Atmos., 110, D18302, doi:10.1029/2004JD005699, 2005.

Schwesig, D. and Matzner, E.: Pools and fluxes of mercury and methylmercury in two forested catchments in Germany, Sci. Total Environ., 260, 213–223, 2000.

Selin, N. E.: Global biogeochemical cycling of mercury: A review, Annu. Rev. Env. Resour., 34, 43–63, 2009.

Sigler, J. M. and Lee, X.: Gaseous mercury in background forest soil in the northeastern United States, J. Geophys. Res.-Biogeo., 111, G02007, doi:10.1029/2005jg000106, 2006.

Smith, L. M. and Reinfelder, J. R.: Mercury volatilization from salt marsh sediments, J. Geophys. Res.-Biogeo., 114, G00C09, doi:10.1029/2009jg000979, 2009.

Smith-Downey, N. V., Sunderland, E. M., and Jacob, D. J.: Anthropogenic impacts on global storage and emissions of mercury from terrestrial soils: Insights from a new global model, J. Geophys. Res.-Biogeo., 115, G03008, doi:10.1029/2009jg001124, 2010.

Sommar, J., Zhu, W., Lin, C.-J., and Feng, X.: Field approaches to measure Hg exchange between natural surfaces and the atmosphere – A review, Crit. Rev. Env. Sci Tech., 43, 1657–1739, 2013a.

Sommar, J., Zhu, W., Shang, L. H., Feng, X. B., and Lin, C.-J.: A whole-air relaxed eddy accumulation measurement system for sampling vertical vapour exchange of elemental mercury, Tellus B, 65, doi:10.3402/tellusb.v65i0.19940, 2013b.

Song, S., Selin, N. E., Soerensen, A. L., Angot, H., Artz, R., Brooks, S., Brunke, E.-G., Conley, G., Dommergue, A., Ebinghaus, R., Holsen, T. M., Jaffe, D. A., Kang, S., Kelley, P., Luke, W. T., Magand, O., Marumoto, K., Pfaffhuber, K. A., Ren, X., Sheu, G.-R., Slemr, F., Warneke, T., Weigelt, A., Weiss-Penzias, P., Wip, D. C., and Zhang, Q.: Top-down constraints on atmospheric mercury emissions and implications for global biogeochemical cycling, Atmos. Chem. Phys., 15, 7103–7125, doi:10.5194/acp-15-7103-2015, 2015.

Song, X. and Van Heyst, B.: Volatilization of mercury from soils in response to simulated precipitation, Atmos. Environ., 39, 7494–7505, 2005.

St Louis, V. L., Rudd, J. W. M., Kelly, C. A., Hall, B. D., Rolfhus, K. R., Scott, K. J., Lindberg, S. E., and Dong, W.: Importance of the forest canopy to fluxes of methyl mercury and total mercury to boreal ecosystems, Environ. Sci. Technol., 35, 3089–3098, 2001.

Streets, D. G., Hao, J., Wu, Y., Jiang, J., Chan, M., Tian, H., and Feng, X.: Anthropogenic mercury emissions in China, Atmos. Environ., 39, 7789–7806, 2005.

Thom, A. S.: Momentum, mass and heat exchange in plant communities, in: Vegetation and the atmosphere, edited by: Monteith, J. L., Academic Press, New York, USA, 57–109, 1975.

Tong, X., Li, J., Yu, Q., and Lin, Z.: Biophysical controls on light response of net CO_2 exchange in a winter wheat field in the North China Plain, PLoS ONE, 9, e89469, doi:10.1371/journal.pone.0089469, 2014.

USGS: Mineral Commodity Summaries 2015 – Mercury, US Geological Survey, available at: http://minerals.usgs.gov/minerals/pubs/commodity/mercury/mcs-2015-mercu.pdf, last access: September 2015.

Wang, D. Y., He, L., Shi, X. J., Wei, S. Q., and Feng, X. B.: Release flux of mercury from different environmental surfaces in Chongqing, China, Chemosphere, 64, 1845–1854, 2006.

Wang, J., Wang, S., Jiang, J., Ding, A., Zheng, M., Zhao, B., Wong, D. C., Zhou, W., Zheng, G., Wang, L., Pleim, J. E., and Hao, J.: Impact of aerosol–meteorology interactions on fine particle pollution during China's severe haze episode in January 2013, Environ. Res. Lett., 9, 094002, doi:10.1088/1748-9326/9/9/094002, 2014.

Wang, L., Wang, S., Zhang, L., Wang, Y., Zhang, Y., Nielsen, C., McElroy, M. B., and Hao, J.: Source apportionment of atmospheric mercury pollution in China using the GEOS-Chem model, Environ. Pollut., 190, 166–175, 2014.

Wang, L. T., Wei, Z., Yang, J., Zhang, Y., Zhang, F. F., Su, J., Meng, C. C., and Zhang, Q.: The 2013 severe haze over southern Hebei, China: model evaluation, source apportionment, and policy implications, Atmos. Chem. Phys., 14, 3151–3173, doi:10.5194/acp-14-3151-2014, 2014.

Wang, S., Zhang, L., Wang, L., Wu, Q., Wang, F., and Hao, J.: A review of atmospheric mercury emissions, pollution and control in China, Front. Environ. Sci. Eng., 8, 631–649, 2014.

Wang, Z., Zhang, X., Xiao, J., Ci, Z., and Yu, P.: Mercury fluxes and pools in three subtropical forested catchments, southwest China, Environ. Pollut., 157, 801–808, 2009.

Wen, L., Chen, J., Yang, L., Wang, X., Xu, C., Sui, X., Yao, L., Zhu, Y., Zhang, J., Zhu, T., and Wang, W.: Enhanced formation of fine particulate nitrate at a rural site on the North China Plain in summer: The important roles of ammonia and ozone, Atmos. Environ., 101, 294–302, 2015.

Wesely, M. L. and Hicks, B. B.: Some factors that affect the deposition rates of sulfur dioxide and similar gases on vegetation., J. Air Waste Manage., 27, 1110–1117, 1977.

Wright, L. P. and Zhang, L. M.: An approach estimating bidirectional air-surface exchange for gaseous elemental mercury at AMNet sites, J. Adv. Model. Earth Syst., 7, 35–49, 2015.

Xiao, Z. F., Munthe, J., Schroeder, W. H., and Lindqvist, O.: Vertical fluxes of volatile mercury over forest soil and lake surfaces in Sweden, Tellus B, 43, 267–279, 1991.

Xin, M. and Gustin, M. S.: Gaseous elemental mercury exchange with low mercury containing soils: Investigation of controlling factors, Appl. Geochem., 22, 1451–1466, 2007.

Yang, Y. K., Zhang, C., Shi, X. J., Lin, T., and Wang, D. Y.: Effect of organic matter and pH on mercury release from soils, J. Environ. Sci.-China, 19, 1349–1354, 2007.

Zhang, H., Lindberg, S. E., and Kuiken, T.: Mysterious diel cycles of mercury emission from soils held in the dark at constant temperature, Atmos. Environ., 42, 5424–5433, 2008.

Zhang, L., Blanchard, P., Gay, D. A., Prestbo, E. M., Risch, M. R., Johnson, D., Narayan, J., Zsolway, R., Holsen, T. M., Miller, E. K., Castro, M. S., Graydon, J. A., Louis, V. L. St., and Dalziel, J.: Estimation of speciated and total mercury dry deposition at monitoring locations in eastern and central North America, Atmos. Chem. Phys., 12, 4327–4340, doi:10.5194/acp-12-4327-2012, 2012.

Zhang, L., Wang, S. X., Wang, L., and Hao, J. M.: Atmospheric mercury concentration and chemical speciation at a rural site in Beijing, China: implications of mercury emission sources, Atmos. Chem. Phys., 13, 10505–10516, doi:10.5194/acp-13-10505-2013, 2013.

Zhang, Y. Q., Liu, R. H., Cui, Y. Q., Zhou, J. P., and Wang, Y.: The characteristic analysis of atmospheric mercury during haze days in Qingdao, China Env. Sci., 34, 1905–1911, 2014.

Zhou, J., Feng, X., Liu, H., Zhang, H., Fu, X., Bao, Z., Wang, X., and Zhang, Y.: Examination of total mercury inputs by precipitation and litterfall in a remote upland forest of Southwestern China, Atmos. Environ., 81, 364–372, 2013.

Zhu, J. S., Wang, D. Y., Liu, X. A., and Zhang, Y. T.: Mercury fluxes from air/surface interfaces in paddy field and dry land, Appl. Geochem., 26, 249–255, 2011.

Zhu, W., Sommar, J., Lin, C.-J., and Feng, X.: Mercury vapor air-surface exchange measured by collocated micrometeorological and enclosure methods – Part I: Data comparability and method characteristics, Atmos. Chem. Phys., 15, 685–702, doi:10.5194/acp-15-685-2015, 2015a.

Zhu, W., Sommar, J., Lin, C.-J., and Feng, X.: Mercury vapor air-surface exchange measured by collocated micrometeorological and enclosure methods – Part II: Bias and uncertainty analysis, Atmos. Chem. Phys., 15, 5359–5376, doi:10.5194/acp-15-5359-2015, 2015b.

Zhu, Z., Sun, X., Zhao, F., and Meixner, F. X.: Ozone concentrations, flux and potential effect on yield during wheat growth in the Northwest-Shandong Plain of China, J. Environ. Sci.-China, 34, 1–9, 2015.